Evaluating airborne fluxes of reactive nitrogen compounds over the marine boundary layer: from eddy covariance to wavelet transform

Qiaoyun Peng

A thesis

submitted in partial fulfillment of the

requirements for the degree of

Master of Science

University of Washington

2019

Committee:

Joel Thornton

Lyatt Jaeglé

Christopher Bretherton

Program Authorized to Offer Degree:

Atmospheric Sciences

University of Washington

Abstract

Evaluating airborne fluxes of reactive nitrogen compounds over the marine boundary layer: from eddy covariance to wavelet transform

Qiaoyun Peng

Chair of the Supervisory Committee:
Professor Joel Thornton
Department of Atmospheric Sciences

Reactive nitrogen compounds (Nr) have different fates in the atmosphere due to differences in the governing process of chemical transformation, physical transport and deposition. Quantifying dry deposition of critical Nr including N_2O_5, HNO_3, and $ClNO_2$ is important for assessing their atmospheric lifetime and potential impacts on NOx cycling and ecosystems. However, little is known quantitatively and qualitatively about surface-atmosphere exchange of these species, especially under dark wintertime conditions. In this study, we use a comprehensive dataset from the Wintertime INvestigation of Transport, Emissions and Reactivity (WINTER) campaign to characterize the chemistry, sources, and removal rates of Nr. Employing both eddy covariance and wavelet analysis methods, we quantified exchange velocities and evaluate their validity using turbulence conditions, spectral patterns, and Nr budget constraints. We focus analysis on the wintertime marine boundary layer due to a greater prevalence of active vertical mixing, though evidence for surface layer decoupling is also present in the flux observations, as well as less stringent requirements on measurement frequency. We find that under conditions of strong vertical mixing, exchange velocities for N_2O_5, HNO_3, and $ClNO_2$ were -0.78 cm • s^{-1}, -0.68 cm • s^{-1}, -0.73 cm • s^{-1} on average indicating net deposition, with a range from -4 cm • s^{-1} to 3 cm • s^{-1} and an uncertainty of 30%. A box model of nighttime reactive nitrogen chemistry is able reproduce the observations by invoking the observationally derived deposition velocities. To our knowledge, this is the first full simultaneous measurement and evaluation of N_2O_5, HNO_3, and $ClNO_2$ fluxes from an aircraft using eddy covariance, with which we provided an observation-based framework for assessing the impact of air-surface exchange on the fate of key nitrogen species.

TABLE OF CONTENTS

Chapter 1 : Introduction

Dinitrogen pentoxide (N_2O_5) is a night-time reservoir of NOx and plays a key role in nocturnal tropospheric chemistry. Heterogeneous uptake of N_2O_5 to aerosol has significant effects on the budget of reactive nitrogen species (Nr thereafter) and particulate nitrate formation (reactions R1-R4 listed below). Direct N_2O_5 uptake by particles and fog droplets is an important source of dissolved nitrate (Reimer et al., 2003). Multiple observation studies as well as model predictions suggest that nitrate, an important contributor to exceedances of the $PM_{2.5}$, takes up nearly 30% of particulate mass during winter (Heald et al., 2012). Meanwhile, reactive nitrogen deposition, as a source of nutrient to terrestrial and aquatic ecosystems, can cause cascading effects in coastal pollution, marine ecology and biogeochemical feedbacks. Most chemistry models assume that N_2O_5 uptake proceeds through hydrolysis to produce nitric acid, effectively a terminal sink for nitrogen oxides (Aldener et al., 2006). However, it was shown that in chlorine-laden aerosol, nitryl chloride ($ClNO_2$) production from N_2O_5 uptake is also significant in many locations (Thornton et al., 2010). Understanding the branching between these two pathways is critical in that $ClNO_2$ could be photolyzed the following day, which simultaneously recycles NOx and enhances the oxidative capacity through chlorine radical production. In a Lagrangian sense, this pathway prolongs the lifetime of NOx, extending the transport distance, or, range of pollution (Phillips et al., 2013). Nocturnal loss of N_2O_5 limits the availability of NO_2 for the photochemical production of ozone the following day. Reactive nitrogen chemistry may differ substantially in winter with different aerosol composition resulting from shifts in thermodynamic equilibrium of ammonium nitrate, which also leads to changes in N_2O_5 heterogeneous uptake (Mentel et al., 1999; Bertram and Thornton, 2009). These processes have potentially important consequences for air quality and human health particularly in polluted coastal regions but still remain elusive. Therefore, the fate of N_2O_5 and its reaction products needs to be more thoroughly investigated.

(R1) $NO_3 + NO_2 + M \rightleftharpoons N_2O_5$
(R2) $N_2O_5 + H_2O(het) \longrightarrow 2HNO_3$
(R3) $N_2O_5 + Cl^{-}(het) \longrightarrow ClNO_2 + NO_3^{-}$
(R4) $ClNO_2 \overset{hv}{\rightarrow} Cl\cdot + NO_2$

For the fate of reactive nitrogen species, not only is the heterogeneous chemistry important, but the deposition or accumulation depending on turbulent transport also has a significant impact. Quantifying deposition of critical NOz species (the difference between NOy (sum of all odd-nitrogen compounds) and NOx) is important for assessing their overall fate and potential impacts on various ecosystems.

Currently, little is known about the relative importance between N_2O_5 uptake to aerosol and its deposition to ground, which may be a controlling factor for the atmospheric lifetimes and mixing ratios of reactive nitrogen species (WINTER white paper). N_2O_5 is highly reactive, and is supposed to deposit at a rate similar to that of HNO_3, but strong suppression of vertical mixing at night over land might inhibit the nocturnal deposition and diminish its overall importance on a boundary layer average. However, Huff measured N_2O_5 deposition over snow in Fairbanks to be on the order of 1 $cm \bullet s^{-1}$, which represents at least 1/8 of the total chemical removal of N_2O_5 near the ground (Huff et al., 2011). During winter nights, sufficient vertical mixing is expected in the marine boundary layer downwind of coasts as the structure of cold continental air over warmer water facilitates convective flows. Further, winter HNO_3 is tied more strongly to N_2O_5, and deposition fate of HNO_3 is likely to be more tied to N_2O_5 fate accordingly. It is thus critical to understand the interplay between reactive nitrogen chemistry and pollutant transport to assess the importance and nature of the various processes involved.

Large uncertainties in exchange velocity yield large uncertainties in modelled ambient concentrations, yet very little information is available to examine the vertical exchange of reactive nitrogen species, partly due to a lack of direct observations. Meanwhile, the limited observations are skewed to summertime periods, despite the fact that the significance of N_2O_5 is likely higher in winter due to the colder and longer nights. As a result, our ability to analyze surface-atmosphere exchange of Nr and other trace gases is inadequate, and the major limitation has been the lack of availability of fast analyzers for reactive nitrogen compounds. Additionally, up to now, most flux observations involving reactive nitrogen compounds are confined to ground-based, continuous but local measurements (Ammann et al., 2012; Geddes and Murphy, 2014; Baldocchi, 2014). These provide a good basis for temporal integration, but may not be representative of the larger regional context. Airborne flux measurements, on the other hand, can provide greater spatial coverage over time periods of a few hours. It is also able to characterize a wide range of ecosystems at regional scale with a single measurement package if combined with certain spectral methods,, helping to bridge the gap in modelling the dynamics of reactive nitrogen at model-relevant scales (1 – 100 km) (Sifuzzaman et al., 2009).

In this paper, we address some of the above questions by presenting observations of reactive nitrogen species and other trace gases at polluted urban areas in Northeastern US during the Wintertime Investigation of Transport, Emissions, and Reactivity (WINTER) campaign. The overarching goal of this study was to determine the direction and magnitude of fluxes on different surfaces (i.e. aerosol, land or sea), and to investigate the impact of possible source and sink mechanisms within a constrained box model. We apply wavelet analysis methods to quantify the turbulent flux and exchange velocity for different gases, and use odd oxygen budget closure as well as a simple box model to evaluate whether the measured exchange velocities are reasonable estimates of dry deposition velocities. The results from this paper contribute to a deeper understanding of production and loss of reactive nitrogen species, associations of vertical transport with meteorological conditions, and model representation of trace gas exchange.

Chapter 2 : Data and Methodology

2.1. WINTER campaign overview

Wintertime INvestigation of Transport, Emissions, and Reactivity (WINTER) is a wintertime aircraft-based field campaign using the NSF/NCAR C-130 to investigate reactive nitrogen chemistry over the northeastern United States. It included comprehensive observations of reactive nitrogen species and other trace gases (e.g., O_3, SO_2, etc) from airborne platforms at a sampling frequency of 2 Hz. Ancillary measurements including aerosol size distribution, 3-D winds along with meteorological data were also recorded. This allowed us to investigate the Nr sources and sinks on landscape and regional scales with direct flux observations, for which there is little, published field data.

2.2. CIMS Instruments

Reactive nitrogen species including N_2O_5, $ClNO_2$, and HNO_3 were measured by the UW High-Resolution Time of Flight Chemical Ionization Mass Spectrometer (HR-ToF-CIMS). I^- reagent ion was used to detect Nr as I^-Nr adduct. Descriptions of the sampling protocol, characteristics of the instrument and an overview of the observations has been published elsewhere (Lee et al., 2014).

2.3. Flux Calculation

A major aspect of this paper is to apply the airborne vertical fluxes derived from eddy covariance and wavelet approaches to evaluate the rate of exchange for key Nr. The following is a brief introduction of both methods.

2.3.1 Eddy covariance

Eddy covariance (EC thereafter) is the most direct and robust method of quantifying the exchange of compounds between the atmosphere and surface (Baldocchi et al., 1988; Moncrieff et al., 1997). Simultaneous measurements of the mixing ratios and vertical wind speeds at high time resolution during WINTER enables flux calculations. We averaged all relevant measurements into 1 Hz time series for convenience. Before computing the eddy flux, spikes were removed and all data were conditioned by 10-min moving average detrending to remove changes in scalars owing to the effects of varying sampling conditions. The turbulent flux (*F*) is calculated as the covariance between the vertical wind velocity (*w*) and gas concentration (*c*) within a period (typically 30 minutes) encompassing n measurements, as shown in Eq. 1 below where the overbar denotes the time average and the primes denote fluctuations from the mean. By convention, the flux is regarded as emission when the covariance is positive and deposition if negative.

(Eq. 1) $\mathrm{F} = \overline{w'c'} = \frac{1}{n}\sum_{i=1}^{n}(w_i - \bar{w})(x_i - \bar{x})$

Flux is less susceptible to errors relative to scalar concentrations since systematic errors in concentration data would not propagate into the covariance calculation. However, adherence to stringent meteorological and site-specific criteria is required, which will be detailed in the following sections. We averaged qualified fluxes into 15-minute chunks to minimize concentration trends within the flux periods while retaining adequate sensitivity to relatively low frequency eddies (Schobesberger et al., 2016). The applicability of this approach hinges on the stationarity and horizontal homogeneity of the region over a long enough time scale. In cases where the premises do not hold, flux values become dubious.

2.3.2 Wavelet

Wavelet, often seen as “mathematical microscopes” in time, is an approach to localize the importance of a given frequency scale in time by expanding the time series into a time-frequency domain. Due to this feature, wavelets allow decomposing various turbulent fluxes into different frequency contributions without necessarily neglecting flux contributions from periods longer than the averaging interval or losing time localization. It uses a parametric basis (we used Morlet wavelet in the paper) which could be translated or contracted to extract the phase and frequency information of a time series.

One striking advantage of the wavelet method is that it relaxes sampling requirements and could be used in heterogeneous land cover and nonstationary conditions, which is not possible in eddy covariance methods. Furthermore, the application of wavelet transforms permits resolving fluxes down to scales of ~1 km, as well as providing detailed frequency components evolution.

In this study, we applied the wavelet method as the primary tool to compute the turbulent fluxes. If the result is comparable to that derived from EC method, it confirms the validity of the measurements as wavelet is a mathematically independent way from EC. Otherwise we take the wavelet flux for further analysis as EC fluxes might suffer from heterogeneous or nonstationary artefacts.

2.4. Quality assurance

Eddy Covariance fluxes must undergo a rigorous quality assessment to ensure the validity of the results. During measurements, lots of complicating factors might limit the applicability of the acquired data, especially in winter nights when vertical mixing is suppressed. Airborne measurements in the turbulent boundary layer are particularly prone to ‘contaminations’ of aircraft movements and vibrations. Non-stationarity of the atmosphere along the flight path adds to the uncertainty (Lenschow 1986). Therefore, it is essential to use a proper strategy to ‘decontaminate’ the observed data series. Following Burba and Anderson (2014), we adopted a series of quality check standards for flux quantification including despiking, detrending, coordinate rotation, etc. No density corrections are needed here since the CIMS measures the mixing ratio of a species in the atmosphere rather than the absolute concentration (Webb et al., 1980). Further processing steps are illustrated below.

2.4.1 Lag time determination

Flux quantification entails precisely synchronized measurements of vertical wind speed and scalars at high accuracy and sampling rate. However, measurement of different gases aboard might be subject to varying delay time in the tubing due to their different ‘stickiness’ to the wall and cause a lag between these signals and scalars acquired by other instruments. Empirically, we correct this lag time of trace gas signals by shifting their time series scan by scan against that of vertical wind speed and running a circular correlation analysis of the signals for selected legs with sufficient fluxes. The lag time is determined as the time corresponding to the absolute maximum (peak) of the correlation function within a physically possible range (here -10–10 s). We did this analysis for all gases of interest and found their lag time to be fairly uniform and constant with time during the flights. In RF 1, the covariance for sonic temperature T with vertical wind were maximized at a lag time of 0 as expected (shown in Figure 2.1). At a time resolution of 1 Hz, the lag time for $w'[HCOOH]'$, $w'[HNO_3]'$ and $w'[N_2O_5]'$ was determined to be

6 s. Therefore, we applied the derived lag time from each measurement phase to quantify the airborne fluxes.

2.4.2 Turbulence threshold

The first step here is to determine the boundary layer height above which the air would be detached from the surface and thus should be exempted from flux analysis. We looked at the vertical gradients of potential temperature which is an indicator of static stability, and it turns out that it was neutral to slightly unstable most of the time in nocturnal marine boundary layer (Figure 2.2). We then retrieved the boundary layer height by manually selecting the altitude at which the potential temperature shows large changes with a subsequent rise to be the top of the planetary boundary layer (PBL). Hereafter, only data within the PBL are retained for flux analysis.

The degree of vertical mixing greatly complicates the understanding on nocturnal Nr chemistry. So, the next step is to filter out the fluxes under low turbulence or stable conditions when the exchange between atmosphere and surface is insufficient. We need to ensure there is enough turbulence in the measurement to gain confidence in the results. Friction velocity, or u*, is a measure for the wind shear and thus wind generated turbulence derived from measurements of horizontal and vertical wind speed (see Eq. 2).

(Eq. 2) $u^* = \left[\overline{(u'w')}^2 + \overline{(v'w')}^2\right]^{1/4}$

In Fig. 2.3, we looked at how sensible heat flux varies with u*. By visually inspecting the trend, we clearly see that the fluxes tend to flatten out at high enough u* while showing a large scatter when u* is low. The large uncertainty associated with low u* (strong stabilities) might be caused by the increase in relative contributions of heterogeneity at stable conditions (Vickers et al., 2010). Only when fluxes become independent of friction velocity, turbulent mixing is deemed sufficient to not result in a systematic bias of night-time fluxes. Therefore, we set a lower limit for the friction velocity using this method and filter out those below the threshold to get meaningful flux values. The criteria above filtered out less than 7% of our raw data.

2.4.3 Stationarity

Fluxes determined by Eq. 1 are valid if the eddies remain unchanged during the transport to the measurement sensor (Taylor hypothesis, see e.g. Stull, 1988). That is, the scalar and vertical wind velocity time series and their covariance do not vary much over time. In practice, the stationarity test by Foken and Wichura (1996) assesses how much the covariance deviates (in %) from perfect stationarity by comparing the mean covariance calculated from shorter sub-periods (typically six 5 min periods) to the 30-min average. In our case, we adopt a less strict standard considering the volatile nature in airborne measurements. The average flux derived from three consecutive 5-min sub-periods was compared to the 15-min eddy flux during the same time window. Only the legs with lower than 30% deviations were saved for further flux analysis. Otherwise, if their mean value differed from the full period flux by more than 30%, i.e., if

$$\text{(Eq. 3)}\ 1 - \left|\frac{\overline{<w'x'>}_{sub-period}}{<w'x'>_{full\,period}}\right| > 0.3$$

the flux was designated non-stationary and discarded in eddy covariance processing.

2.4.4 Spectral analysis

Fluxes are subject to various systematic errors depending on the measurement system and processing approach. Moreover, the moving platform may additionally influence the spectral quality in the case of airborne measurements. High-frequency concentration fluctuations may be attenuated by sensor separation, line averaging within the instrument tube, limited sampling frequency and sample mixing and smearing due to wall effects (Lenschow et al., 1991). On the other hand, flux error at the low-frequency end could take place if the averaging interval is inappropriate. If the interval is too long, non-turbulent transfer like mesoscale motions might be incorporated, leading to flux overestimate; if that is too short to capture an adequate ensemble of eddies contributing to turbulent motions, a bias in flux happens due to missed input from larger eddies. Proper spectral correction helps separate "locally meaningful" flux from background trends and oscillations.

To investigate the accuracy of airborne trace gas flux measurements, we used a spectral analysis to compare Nr fluxes with the well-known behavior of heat fluxes. Sensible heat flux is assumed to be undamped since there is no delay between temperature and velocity measurement. According to the similarity theory (Kaimal et al., 1972), cospectra of all the scalars in the inertial subrange are similar and should follow the theoretical drop-off of -5/3. Here, we examine the power spectra for multiple scalars of 15-minute long flight legs at 300 m above ground. This 15-min average interval is chosen as a trade-off between the stationarity and inclusivity requirements. The measurements were taken over the ocean in a convective marine boundary layer. In Fig. 2.4, we showed the power spectrum of different scalars in log-log space, all of which nicely follow the -5/3 decay in the range of dominant eddy transport in the convective boundary layer. Beyond about 0.03 Hz, a shallower spectral drop-off due to dampening in the tubing is visible for HNO_3. This attenuation is expected as the laminar flow in the sampling tubes and the 'sticky' nature of HNO_3 will cause smearing of high-frequency fluctuations. The flux attenuations at high frequencies were calculated by comparison with the sensible heat flux cospectra, and result shows that 90 - 96% of the Nr flux occurs at frequencies lower than 1 Hz, confirming that CIMS was fast enough to capture the dominant flux-carrying eddies and high-frequency attenuation introduces only a small systematic bias to flux. Due to this small error and the difficulties in predicting spectra for reactive trace gases, we do not apply a correction to the fluxes.

2.4.5 Flux uncertainty quantification

Random error is likely more important in fluxes as compared to systematic error as the measurement and quantification system is optimized. Also, since the correlation between mixing ratios and vertical wind variations is usually low, their covariance (i.e. fluxes) is typically less subject to random noise than mixing ratios (Smeets et al., 2009). Random errors of instrument calibration (σ_{inst}) were calculated after Wolfe et al. (2009), as shown in Eq. 4 below.

(Eq. 4) $\sigma_{inst} \cong \sigma_w \cdot \sigma_n \cdot \sqrt{\frac{\Delta t}{T}}$

where σ_w is the standard deviation of the vertical wind speed measurements, Δt the measurement time resolution (1 s) and T the length of the respective flux period. The standard deviation for instrumental noise, σ_n, was described by the Poisson variance, i.e. the square root of the average signal. Higher values are generally obtained during nighttime, and lower values (3% relative uncertainty on average) during daytime. The average instrument uncertainty of 22% dominates the total uncertainty for our derived Nr fluxes.

The uncertainties for each discrete flux sampling period were also determined empirically by calculating the covariance between vertical wind speed and CIMS signal (w'[Nr]') at lag times significantly longer than the calculated lag time (eg. at ± 21 to 40 s). These uncertainties, σ_{cov}, were usually larger than σ_{inst}, with a mean and standard deviation of 20% ± 15%. With consideration of median values of σ_{cov} and σ_{inst}, we conservatively estimated a total uncertainty of typically about ±30%.

2.5 Figures

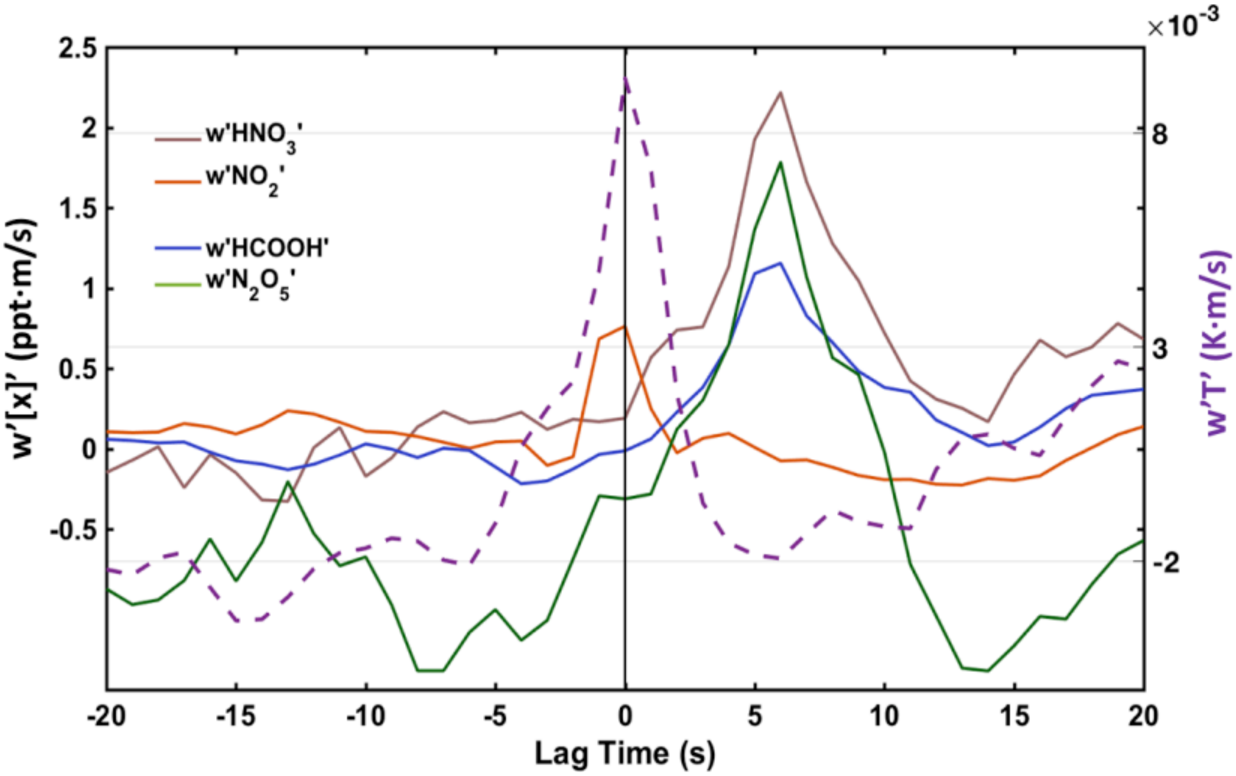

Figure 2.1. Cross correlation functions (in absolute values) of airborne vertical fluxes of HNO_3 (brown), NO_2 (red), formic acid (blue), N_2O_5 (green) corresponding to the left axis, and the sensible heat flux (dashed purple) corresponding to the right axis in RF 1.

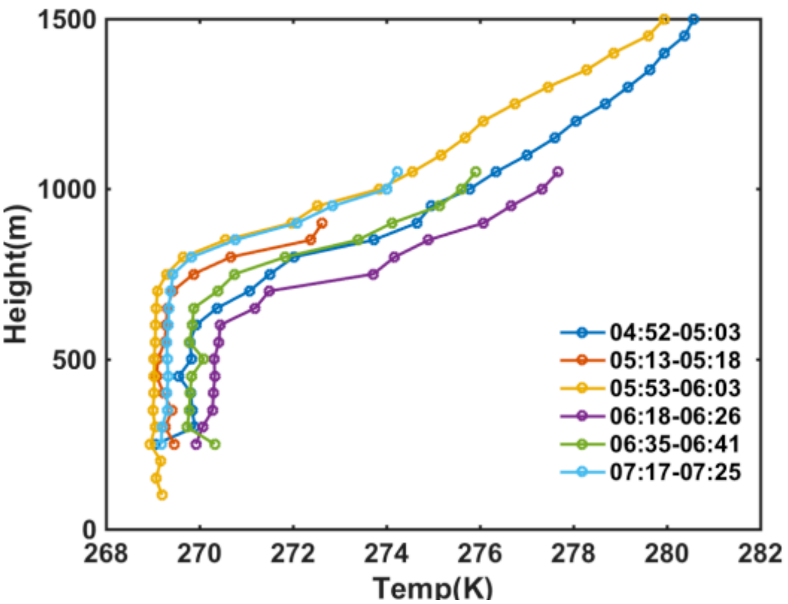

Figure 2.2. Temporal shift of vertical profiles of potential temperature in RF 8. Legend shows the corresponding vertical sampling time period (local time).

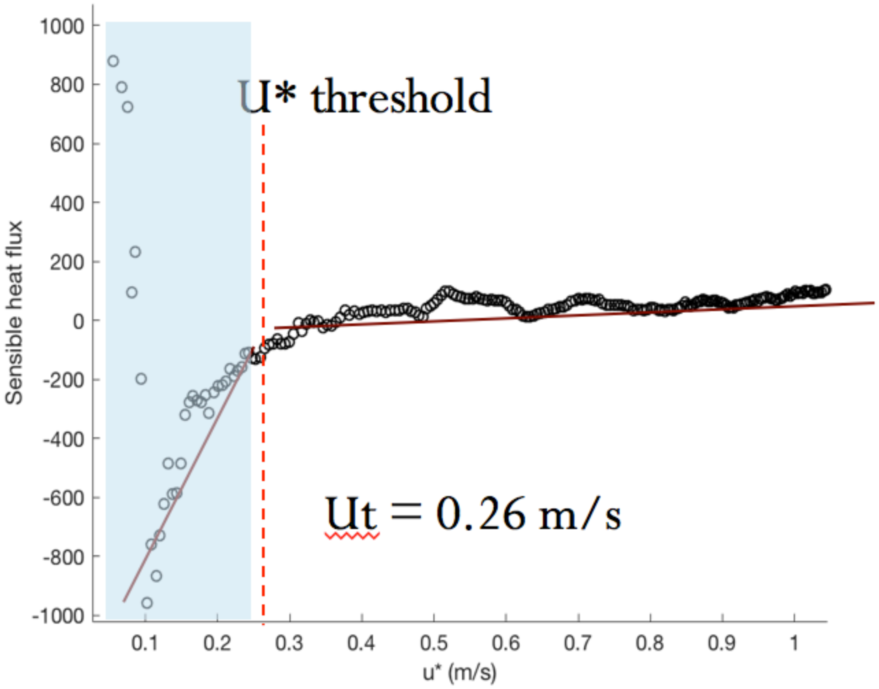

Figure 2.3. Sensible heat flux variations with friction velocity (u*) in RF 1. The u* threshold is selected where the sensible heat flux starts to stabilize.

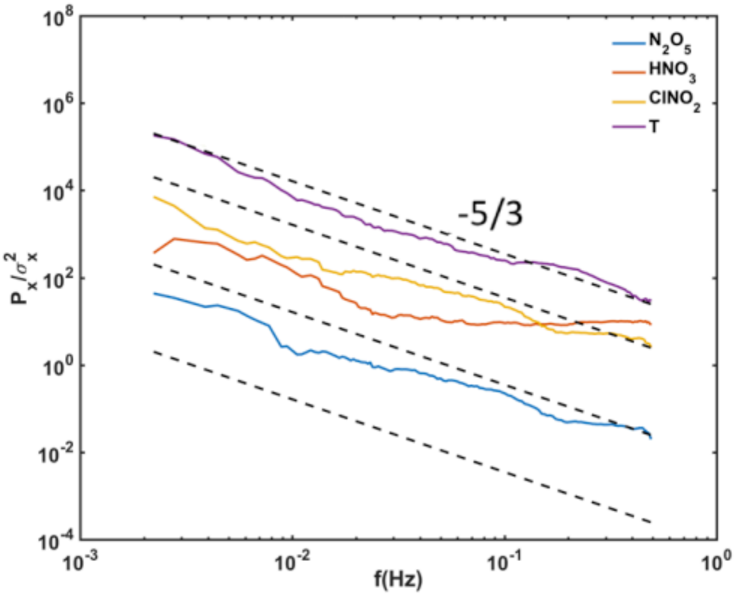

Figure 2.4. Power spectrum density for N_2O_5, HNO_3, $ClNO_2$, and temperature in RF 1. The theoretical drop-off of -5/3 (black dashed) is also plotted for reference.

Chapter 3 : Wavelet and Eddy Covariance Flux Analysis

3.1 Wavelet decomposition and discretized fluxes

Although the eddy covariance method has been proven as the highly accurate standard for flux calculation, wavelet analysis has two advantages: first, wavelet decomposition removes the need to block-average flight sub-sections and gives fine surface resolution that is essential when surveying rapid transients (Torrence and Compo, 1998). Second, wavelet transform relaxes sampling conditions as it does not require surface homogeneity, and could be applied to time series containing non-stationary power (e.g. Terradellas et al., 2001; Strunin and Hiyama, 2004). Therefore, we used wavelet transforms of the high-frequency measurement data to improve spatial/temporal localization of the flux observations. Here, we examined the fluxes of various reactive nitrogen species over urban and coastal regions with continuous wavelet transform methods, helping understand the nature of non-stationary, dynamic aspects of trace gas signals.

3.1.1 Example of Continuous wavelet transform (CWT)

We constructed the wavelet cross-scalograms with two scalar time series (vertical wind velocity and N_2O_5 concentration in this case) which will expose their common power in the time-frequency space. By looking at the cross-scalogram it is possible to determine where in the wavelet period (inverse of frequency) and in time/space the flux contribution occurs, enabling the visualization of the local covariance between the time series at each scale. A wavelet coefficient can be either positive or negative in different scales at a given point in time, reflecting eddies of different sizes moving instantaneously upward or downward. The figures are very informative and allow the locations of so-called events (hotspot zones) to be traced. However, the interpretation of the scalogram demands attention to the original time series as times of high common power may result from either high power in both time series or from extreme high power in one time series, in addition to errors associated with edge effects (Maraun and Kurths, 2004). The wavelet flux was obtained by integrating over the cross-scalograms over a sliding one-minute window.

As an example, Figure 3.1 (middle panel) shows a wavelet cross-scalogram of N_2O_5 fluxes in RF 8. Red areas denote positive power; blue areas negative. Power is bias-corrected (frequency-weighted) as suggested by Liu et al. (2007). The area under the dashed curve indicates the cone of influence (COI) which is the spectral region where wavelet coefficients may contain artefacts due to edge effects. Instead of directly excluding the part falling outside the COI, each of the ends of the time series are padded with zeros and excluded afterward, so the results are not affected by the COI. As shown in the middle panel of Fig. 3.1, the scattering field near the top of the plot is contributed primarily by noisy background turbulence. As the scale increases, the distributions tend to be organized into discrete plume-like structures near the time scale of ~15 - 50 s. This middle part is likely to be a region where boundary layer circulations interact with organized structures. The strength and continuity of the interactions are associated with the turbulent exchange of gases and energy. At the bottom of the scalogram, the large positive (red color) and negative (blue color) centers correspond to the low-frequency trends on the order of tens of minutes (~500 s) which could be associated with large eddies or thermal plumes. There is clear negative power at wavelet scales between 0 and 128 s. At typical aircraft speed of 50 m/s, these features would correspond to spatial scales on the order of 6.4 km and exhibit local sink. Fluxes driven by these high-frequency fluctuations (turbulence) are inherently local in nature, whereas fluxes driven by low-frequency fluctuations (< 0.001 Hz) are associated with large-scale meteorological phenomena.

Similar to Fourier spectral analysis introduced in section 2.4.3, wavelet global co-spectra through integration of cross-scalograms in time/space domain allow a separation between different types (frequencies) of flux and estimation of the fractional contribution to the net flux. As shown in Fig. 3.2, 90% of the cospectral power for N_2O_5 fluxes in RF 8 occurs between 0.01 – 0.1 Hz. The Fourier cospectrum shows overall similar features but with more noise. The ogive indicates that 99% of flux-carrying eddies occur below 0.4 Hz, inferring that high frequency spectra correction was not needed, with a low contribution to the calculated flux. Thus, the 1 Hz data used in this analysis meets the inclusivity requirement, and faster measurement, while desirable, is not strictly necessary. The generally good quality of fluxes arises from a combination of factors such as high instrument sensitivities, slow aircraft speeds and proximity to the source by flying at low altitudes (e.g., 300 m) and lack of spectral interferences (e.g., from propellers).

Cospectra calculations for other Nr species and sensible heat flux were also carried out. For scales lower than 0.004 Hz, the flux contributions for all scalars were almost zero. From 0.004 Hz to higher frequencies, fluxes increase significantly, which shows a strong contribution of small-scale turbulence to the total transport.

3.2 Exchange velocity and flux for Nr

As both a source and sink of many atmospheric species, surface-atmosphere exchange represents a critical link between the atmosphere and the earth system. The overall goal of this paper is to evaluate the exchange velocity of reactive nitrogen species, and elucidate the pathways of production and loss. Being able to directly and simultaneously measure the concentrations of the N_2O_5-HNO_3-$ClNO_2$ triad and 3-D wind speed, we derived the trace gas exchange velocities over different underlying surfaces at different time of day. We calculate the exchange velocity (V_{ex}) at one altitude by dividing the turbulent flux (F) by the concentration of the trace gas (C): $V_{ex} = \frac{F}{C}$. Note that deposition velocity (V_{dep}) is the negation of exchange velocity (V_{ex}) by definition. V_{ex} represent net surface-atmosphere exchange, and negative values indicate that emissions were exceeded by uptake at the measurement plane or that concentrations aloft were elevated, perhaps because of airborne sources or elevated plumes; positive values denote opposite processes with more updrafts than downdrafts or possible sinks aloft. The potential temperature gradients in flights over marine boundary layer allow us to infer that the area is not subject to strong surface inversions. This is further emphasized in the vertical velocity variance (σ_w), predominantly in the range of 0.2 - 0.6 $m \cdot s^{-1}$. Therefore, we assume that the fluxes are meaningful and faithfully reflect the vertical transport.

Here, we discuss the direction and magnitude of the exchange for each individual Nr and hopefully shed light on their interaction mechanisms. Spatially variable distributions of deposition can be assessed from aircraft measurements, as shown in the 1-min resolved observations in Figure 3.3. High upward Vex spatially coincide with the portion of the flight leg where the airplane flew over the plume intersections. This phenomenon might be due to the venting of previously accumulated and advected HNO_3 that was trapped below the measurement height under low turbulence conditions. The spatial-temporal variability of exchange velocities for reactive nitrogen compounds demonstrates the need for sufficient measurements to obtain meaningful flux results for the large span of environmental conditions. Thus, to understand the range of Nr fluxes, statistical analyses of CWT instantaneous fluxes are performed as follow.

In Figure 3.4 – 3.6, we showed the frequency distribution of wavelet-derived exchange velocity for all three reactive nitrogen compounds for flights sampled within the marine boundary layer. Significant in-flight and cross-flight variabilities are found in the exchange velocity distributions, which may be related to regional differences in factors such as sea surface temperature, boundary layer mixing, etc, yet their ranges are similar (approximately -4 – 3 cm • s^{-1}). It is clear that the histograms all show a negative bias, indicative of a net downward flux over the ocean surface. Some periods associated with positive V_{ex} are also obtained, possibly due to the accumulation of Nr pools when the surface layer was decoupled from the air above, or simply geophysical variability of the instantaneous flux measurements. In the following sections, we elaborate on the V_{ex} distribution during WINTER and literature values for N_2O_5-HNO_3-$ClNO_2$ triad.

3.2.1. Dinitrogen pentoxide (N_2O_5)

The nighttime deposition is an important loss pathway of N_2O_5 and it is therefore important to quantify the deposition velocity for understanding the fate of nitrogen species in different environments. However, to our knowledge, there are very few reported deposition velocities for N_2O_5. Modelling studies have assumed N_2O_5 deposition velocities of up to 2 cm • s^{-1} in urban areas (Sander and Crutzen, 1996). Extension of laboratory determined reaction rates and equilibrium constants to the air−sea interface suggests that N_2O_5 deposition to the ocean should be rapid (Kim et al., 2014). Using eddy covariance method, Kim measured the mean deposition velocity of N_2O_5 to be 1.66 ± 0.60 cm • s^{-1} at an average wind speed of 9 m • s^{-1} over the air-sea interface. Huff measured downward directed deposition velocity of N_2O_5 towards the snowpack surface to be on the order of 1 cm • s^{-1} and determined that the average was 0.59 ± 0.47 cm • s^{-1} which represents at least 1/8 of the total chemical removal of N_2O_5 near the ground (Huff et al., 2011).

As seen in Fig 3.4, we displayed the wavelet-derived N_2O_5 V_{ex} frequency distribution for all ocean flights during WINTER, and it turns out that N_2O_5 mostly shows a depositing behavior with flight-average deposition velocity ranging from 0.61 to 1.48 $cm \cdot s^{-1}$. We excluded RF 13 for N_2O_5 deposition analysis since it was a daytime flight and N_2O_5 concentrations were pretty low. Upward fluxes of N_2O_5 were sometimes captured, which may indicate periods of insufficient mixing. This also suggests that if nocturnally deposited N_2O_5 forms a conservative surface reservoir, which can be released later on, a significant fraction of the daytime N_2O_5 source can be explained for the WINTER observations. From a more general perspective, the role of N_2O_5 surface exchange, i.e., its ability to serve as either a reservoir or a sink for NOx, may vary strongly with both time and location. The spatially distinct V_{ex} also highlights the difference in the chemical composition and characteristics of underlying surface.

3.2.2. Nitric acid (HNO_3)

Nitric acid has no known biological emissions to the atmosphere and is highly sticky. It is a challenging compound to measure because of its interactions with instrument surfaces. A further complication in measuring fluxes of HNO_3 is its potentially rapid exchange with its aerosol counterpart (pNO_3^-), resulting in the potential for sources and sinks below the measurement height that alters the fluxes. Many HNO_3 deposition studies have been conducted over the past several decades using various techniques including eddy correlation and profile methods, and its dry deposition velocity encompasses a wide range from -1 to 8 $cm \cdot s^{-1}$ in the literature (Meyers et al., 1991; Farmer et al., 2006; Farmer et al., 2008), and these values are commonly used in global chemical transport models (e.g., Brasseur et al., 1998) and regional models of NOx budgets (e.g., Munger et al., 1999). Farmer and Cohen (2008) reported HNO_3 deposition velocities of 3–4 $cm \cdot s^{-1}$ during winter using eddy covariance measurements but suggested that fast intra-canopy chemistry could influence HNO_3 fluxes, even to the point of reversing its direction. Some authors only provide fluxes of total nitrate ($TN=HNO_3 + NO_3^-$) to avoid possible interference from gas-particle partitioning (Wolff et al., 2010), but the majority of measurements have been reported without taking account of simultaneously evolving thermodynamics. Nguyen et al (2015) determined nitric acid deposition rate of 3.8 ± 1.3 $cm \cdot s^{-1}$ in a temperate forest, consistent with results from resistance modeling performed in the same study.

In WINTER, we observed the average deposition velocity of 0.68 $cm \cdot s^{-1}$ for HNO_3 in ocean flights, which is within the previously reported range. It shows downward flux most of the time, so we assume the ocean surface is likely to be a net HNO_3 sink given the slight alkalinity of seawater. However, apparent HNO_3 emissions or reduced HNO_3 deposition rates have also been observed mostly during the day. The phenomenon implies either a direct emission source (eg. pooling of advected plumes) or a prompt chemical transformation process (eg. aerosol evaporation artefacts). There might be a reduced uptake rate of HNO_3 with height in some cases, as its equilibrium with pNO_3 tends to shift towards retention of particulate nitrate over release of HNO_3 with increasing altitude (lower temperature), which has been reported in the past (Nemitz and Sutton, 2004). Under these conditions, large apparent deposition rates for aerosol NO_3^- or NH_4^+ have been measured. This process converts rapidly depositing gaseous compounds into slowly depositing aerosol species, thereby reducing total N deposition and may also deprecating γ at low temperatures due to the release of nitrate from the particles (Phillips et al., 2016).

3.2.3. Nitryl chloride ($ClNO_2$)

$ClNO_2$ is produced primarily by N_2O_5 uptake on chloride-containing aerosol particles (Behnke et al., 1997; Thornton and Abbatt, 2005; Bertram and Thornton, 2009) or potentially ground surfaces (Lopez-Hilfiker et al., 2012). The a priori estimate for the magnitude and direction of $ClNO_2$ flux over ocean is uncertain depending on the aqueous phase chemical reactions of nitronium ion (NO_2^+) in water (Behnke et al.,1997). Competition between volatilization and aqueous-phase reactions of $ClNO_2$ in the organic-rich sea surface microlayer determines the net surface-atmosphere exchange. Modelling studies by Kim et al (2014) suggests that air-sea $ClNO_2$ exchange is responsive to the chemical composition in the surface ocean – approximately half of deposited N_2O_5 is returned to the atmosphere as $ClNO_2$ when yield $\Phi(ClNO_2)_{ocean} \rightarrow 1$, while all N_2O_5 is terminally lost to ocean when $\Phi(ClNO_2)_{ocean} \rightarrow 0$. As such, $ClNO_2$ exchange velocity shall display large spatiotemporal variability depending on the characteristics of surface. The exchange of $ClNO_2$ with underlying surface could be bidirectional, since the surface sometimes provides a reservoir for the species and allows reemission to the atmosphere while other times being a permanent sink. The potential of surface ocean to be either a source or a sink to $ClNO_2$ is significant for subsequent removal of emitted nitrogen oxides from the atmosphere.

According to Kim et al (2014), $ClNO_2$ displays net deposition at the air−sea interface, suggesting that elevated $ClNO_2$ mixing ratios in the marine boundary layer are sustained primarily by N_2O_5 reactions with aerosol particles. To our knowledge, no further direct measurement of $ClNO_2$ flux or quantitative result on $ClNO_2$ exchange velocity has been reported.

In our study, $ClNO_2$ flux over all ocean flights (we excluded RF 1 and RF 13 here since there were few $ClNO_2$ measurements above the instrument detection limit) exhibits net downward patterns, suggesting that water-side transport and transformations outpaced gas release into air. The flight-average exchange velocity is 0.73 $cm \bullet s^{-1}$ for all marine boundary layer flights. Moreover, we found the exchange velocity of $ClNO_2$ vary almost linearly with that of HNO_3, and they mostly exhibit the same directions in RF 8 (Fig. 3.7). This implies that they are subject to similar source and sink influence. The lack of exchange velocity studies makes it difficult to compare our results to other studies. As such, we will apply a budget analysis of the odd oxygen family in Chapter 4 to help testify if our quantification of Nr exchange rates are reasonable.

The similar flux frequency variability between Nr compounds implies their tight coupling and potentially close relationship to environmental driving variables such as temperature or relative humidity. In other words, variability in forcings at these frequencies may translate into flux variability at concomitant time scales. Empirically, the relative magnitude of the deposition process is expected to be variable based on: (i) location, since underlying surfaces are highly variable in composition, changing the uptake of Nr; and (ii) time of day, since temperature, relative humidity, other meteorological parameters, and chemical composition of the atmosphere will all have diurnal variations.

3.3. Comparison with EC flux

Comparison of fluxes derived by wavelet integration and eddy covariance is an additional quality check for the measured fluxes. Identical values from the two methods were not expected as the EC flux is affected by non-stationarities and inhomogeneities in contrast to the wavelet flux, but the consistency of the results should strengthen their credibility. One important concern is that wavelet coefficients below the COI are disturbed with edge effects and cannot be localized in the scale domain (Mauder et al., 2007). Taking that into account, an important question is how we define the flux that we want to determine, and what scale range we should cover. When integrating only over wavelengths shorter than the COI, the spectral range represented in the flux estimate is smaller, yet integrating over all wavelet coefficients would introduce large uncertainty in flux quantification. In our analysis, all wavelet fluxes were determined by integration of cross-scalograms above the COI, even if we do not cover the full spectral range of atmospheric transport. But with this approach we know which scale and which segment of the flight track flux contributions originate from.

For most survey flight transects, there were no significant differences between EC and wavelet fluxes, as shown in Fig. 3.8. Occasionally, a flux difference by more than 15% was seen on short segments, or over a nonhomogeneous transect, or when the fluxes were close to zero. For example, the large relative difference between the wavelet flux and the EC flux of N_2O_5 can be explained by its low absolute value in RF 1. The generally good agreement between results obtained through different mathematical techniques underscores the confidence in the analysis of aircraft turbulence data obtained over non-homogeneous terrain.

3.4. Comparison with resistance model results

In this section, we investigate the restricting processes in vertical transport of Nr to the surface using GEOS-Chem's current resistance-in-series Wesely scheme (1989). In relation to deposition transport, the boundary layer may be considered to consist of two layers: the fully turbulent layer and the quasi-laminar layer. In this quasi-laminar layer, which is in the immediate vicinity of the surface, the transport is dominated by molecular diffusion. Once at the surface, the chemical, biological and physical nature of the surface determines the reactive losses of the gases. Accordingly, the total resistance that the vertical transport to surface undergoes is a sum of resistances encountered during turbulence, diffusion, and reaction processes, which is known as

R_a, R_b, and R_c, respectively. R_a is the aerodynamic resistance to transfer of a species as a result of atmospheric turbulence in the mixing layer, characterized by roughness length. R_b is the quasi-laminar layer resistance, and R_c is the surface resistance. For trace gases with negligible surface resistance, the deposition velocity is sensitive to the atmospheric resistances (R_a and R_b), which over rough surfaces are usually small (5–10 $s \cdot m^{-1}$). Based on the Wesely scheme, the deposition-limiting conductance (inverse of resistance) determines the upper limit of deposition velocity of Nr on the surface. Currently there are insufficient field data to accurately parameterize R_c and this remains an area of active research in modelling studies. Additionally, one limitation of the resistance formulation is that it is unable to simulate cases of 'emission' or bi-directional fluxes induced by an underlying source, since it assumes that the concentration of the gas at the absorbing surface to be zero. When the assumption is not satisfied (eg. the surface has non-zero concentration), decreased driving force for deposition or an increased surface resistance would be parameterized, yet could not yield a possible direction reversal observed in the measurements.

HNO_3 is highly water soluble and commonly assumed to deposit at the maximum rate permitted by turbulence, i.e. surface resistance (Rc) is negligible (Sutton et al., 2011). In our studies, Nr depositional velocity derived from eddy covariance method could reach their largest depositional potential when the friction is low. Meanwhile, our observed deposition velocities satisfied the upper limit constrained with atmospheric resistances ($V_d \leq 1/(R_a + R_b)$) within uncertainties throughout these measurements. We illustrate the relation between measured V_{ex} and our estimates of resistances for RF 1 in Figure 3.9. Apparently, aerodynamic resistance (R_a), which was likely elevated due to reduced turbulence, exerted the greatest control over N_2O_5 vertical transport efficiency in the marine boundary layer, especially when the wind speed is low. HNO_3 and $ClNO_2$ also exhibits similar patterns. However, there is growing evidence of possible nitric acid ‘emissions’ and $R_c > 0\ s \cdot m^{-1}$ over different surfaces (Neftel et al., 1996; Nemitz et al., 2004; Farmer et al., 2006), implying the possibility of bi-directional exchange or unidentified source and flux mechanisms, while the Nr updrafts we reported above are more likely the result of a stratified air mass in the residual layer mixing upward to the altitude location of the aircraft, instead of an emission of HNO_3 from the surface. Deposition on land may be very different from deposition to water surfaces due to drastically different surface characteristics and convection conditions. More analysis on land-atmosphere exchange is required to improve our understanding on the surface resistance constraints.

3.5. Implications of deposition on nocturnal nitrogen chemistry

The fate of tropospheric N_2O_5 can lead to either net O_3 destruction through HNO_3 formation pathway or irreversible deposition as a nocturnal loss mechanism, or net O_3 production via NO_2 regeneration from N_2O_5 and $ClNO_2$, which serve as NOx reservoirs. N_2O_5 loss rate is highly variable with distinct values for inland and marine aerosols (e.g. Brown et al., 2006; Osthoff et al., 2008). Local atmospheric composition and meteorological conditions may also moderate the importance of deposition. The indirect measurements of N_2O_5 deposition carried out by Huff et al (2011) suggests that on average, about 1/8 of the chemical removal of N_2O_5 arises from deposition of N_2O_5 to snowpack. Apodaca et al. (2008) showed that dry aerosol surface area was insufficient to explain the loss of N_2O_5 observed, suggesting loss to other surfaces also contributes. Recent studies suggest that surface deposition of N_2O_5 could be an important contribution to its nocturnal loss and lifetime (Huff et al., 2011; Kim et al., 2014). In this section, we evaluate the heterogeneous loss rate of N_2O_5 using in situ aircraft observations. We plotted the wavelet 1-min deposition loss rate K_{dep} against measured aerosol surface area, as shown in Fig. 3.10. In this way, N_2O_5 uptake coefficients over the underlying ground, $\gamma_{ground}(N_2O_5)$, could be derived with Eq. 5. From the observation, we found that the majority of the $\gamma_{ground}(N_2O_5)$ data fell in a range of uptake coefficients from 0.001–0.005, slightly lower than its heterogeneous loss to aerosol surface ($\gamma_{aerosol}(N_2O_5) \sim 0.0024$), suggesting that deposition constituted an important part of the total loss.

Many previous field studies derived $\gamma(N_2O_5)$ using the chemical pseudo steady state calculations described by Brown et al. (2003), which may be rendered inappropriate under cold temperatures and high NOx concentrations encountered in winter urban areas since the equilibrium between NO_3 and N_2O_5 can be too slow to approach steady state. In our study, considering the relatively low NO_x concentration (2.31 ppb on average in RF 8), we assume steady state was achieved. Based on this assumption, we regressed the product of N_2O_5 inverse lifetimes and $K_{eq}[NO_2]$ with $\frac{\gamma CSa}{4} K_{eq}[NO_2]$ for both plume 1 and plume 2 (equation 3), as shown in Fig. 3.11.

(Eq. 3) $\tau\ (N_2O_5)^{-1} K_{eq}[NO_2] \approx k(NO_3) + \frac{\gamma CSa}{4} K_{eq}[NO_2]$

We found that there was a significant correlation between the aerosol surface area and $K_{eq}[NO_2]$, which confirms the viability of applying linear fits to Eq. 3 for determination of $\gamma(N_2O_5)$. The good linearity of the fits attests to the steady state assumption, though there is more scattering at larger $[NO_2]$ in plume 2, likely owing to proximity to sunrise. From the nighttime steady state fits, we determined N_2O_5 uptake coefficient (γ) and the pseudo first order loss coefficient of NO_3. γ is 0.0022 for plume 1 and 0.0026 for plume 2, while the strengths of the sinks for NO_3 ($k(NO_3)$) are quite low (approximately zero), consistent with minimal BVOC impact during winter. In this calculation, dry deposition in RF 8 (i.e., uptake by the ocean surface) for N_2O_5 has not been accounted for in the calculated loss rate coefficient γ. Assuming a 500 m depth for the marine boundary layer, and a deposition velocity for N_2O_5 of 1 cm/s, the predicted lifetime with respect to deposition is nearly 14 hours. This loss is comparable to calculated losses due to heterogeneous uptake to aerosol surface with both loss rate coefficients on the order of 10^{-5}, indicating that N_2O_5 concentrations might be equally dependent on both chemical loss and deposition. From box modeling of the WINTER data by McDuffie et al (2018), 2876 individual $\gamma(N_2O_5)$ values were derived with a median value of 0.0135 (+58/-55%) and 4-order of magnitude range. The plume N_2O_5 uptake in RF 8 is on the lower end of this box model derived γ range in WINTER. The analysis assumes that the γ and $k(NO_3)$ within the power plant plumes did not change during the transport. The potential variability in these quantities likely bias the estimates, but using the averaged values is a necessary simplification to best describe the observations.

Deposition losses of N_2O_5 have typically been considered small in comparison to other losses (Stutz et al., 2004; Aldener et al., 2006). At a measurement height of ~300 meters, we could easily quantify the loss coefficient K_{dep} and K_{het} using equation 4 and 5 below:

(Eq. 4) $K_{dep} = \frac{V_{dep}}{Z_{eff}}$

(Eq. 5) $\mathrm{K_{het}} = \frac{\gamma \mathrm{CSa}}{4}$

In Eq. 4, Z_{eff} is defined as the effective height for gas deposition, which relies upon similarity theory. For simplicity and conformity with other studies, here we adopt the average boundary layer height manually determined from measured potential temperature vertical profiles as estimates of Z_{eff}. This gives us a value of 2.90×10^{-5} s^{-1} for K_{dep} of N_2O_5 in RF 8, which is of the same order of magnitude as compared to the heterogeneous uptake coefficient K_{het} in the plume ($3.60x10^{-5}$) and flight average ($7.23x10^{-5}$). Both parameters (K_{dep} and K_{het}) are within the ranges of laboratory and model coefficients. These results indicate that under conditions of shallow boundary layer heights, which is common for winter nights, uptake to the ocean surface is a non-negligible loss pathway and would strongly affect the fate of Nr. However, stratification and reduced mixing of marine air masses within the shallow boundary layer could lead to vertical gradients in N_2O_5 and/or their sources and sinks (i.e. flux divergence) that in turn could complicate the analysis of N_2O_5 sink budgets because of uncertainties in the rates of mixing processes between adjacent, inhomogeneous air masses (Geyer and Stutz, 2004). In this case, measurement at a specific height may not be representative for the overall surface-atmosphere turbulent exchange. These possible effects have not been included in this analysis.

3.6 Figures

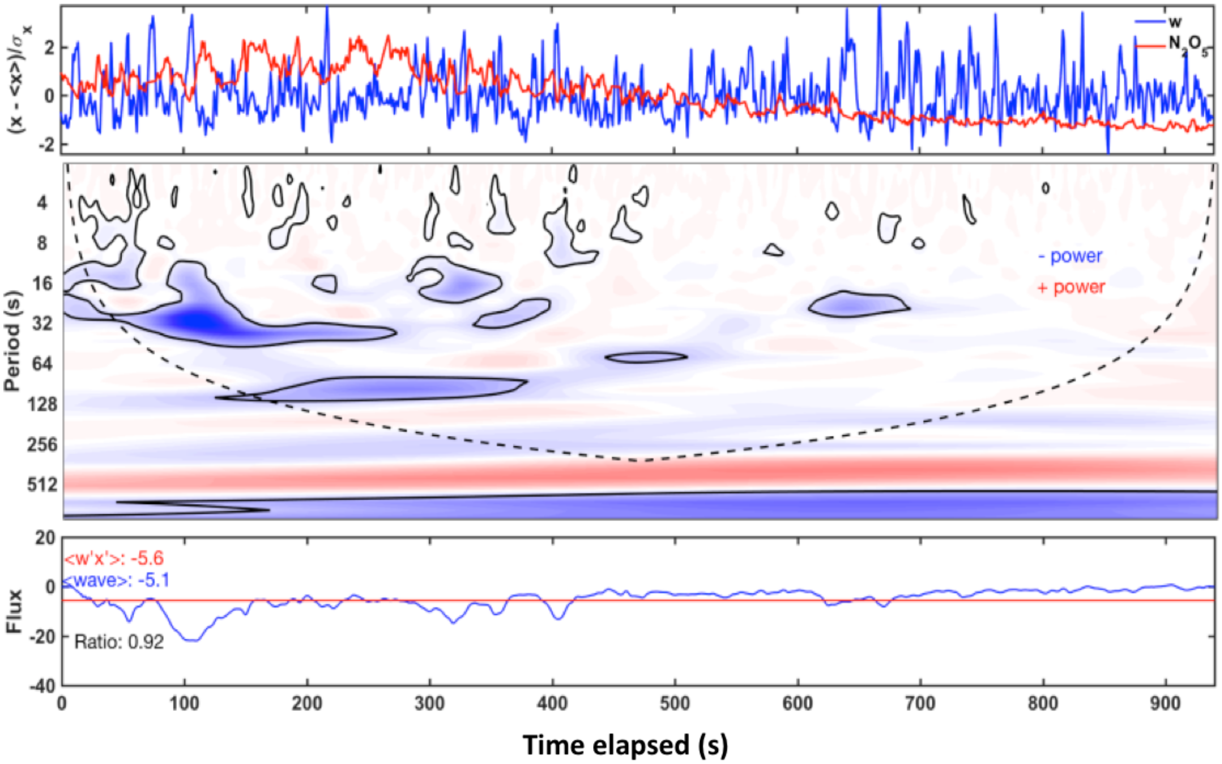

Figure 3.1. Wavelet analysis for N_2O_5 fluxes in RF 8 over ocean. (top) normalized time series for vertical wind velocity (blue) and N_2O_5 concentrations (red); (middle) wavelet cross-scalogram for N_2O_5 fluxes. Blue denotes negative power and red denotes positive power; (bottom) Comparison between ensemble eddy covariance (red) and wavelet (blue) derived flux values.

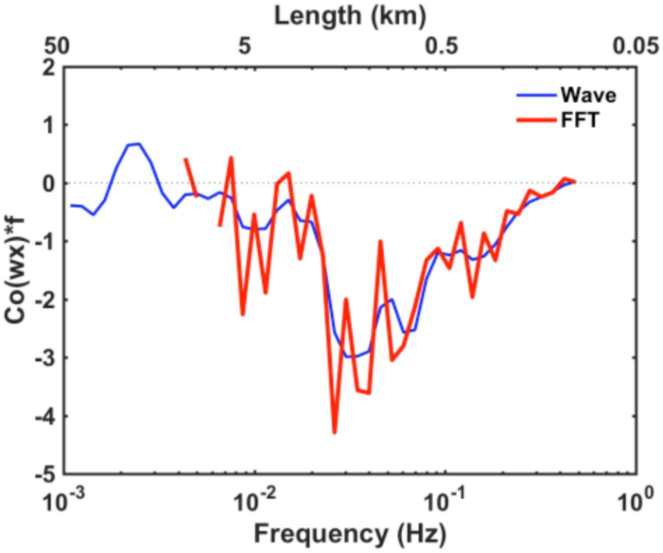

Figure 3.2. Global wavelet cospectra for N_2O_5 flux derived from wavelet method (blue) or Fourier transform (red) in RF 8 during the same period as in Figure 3.1.

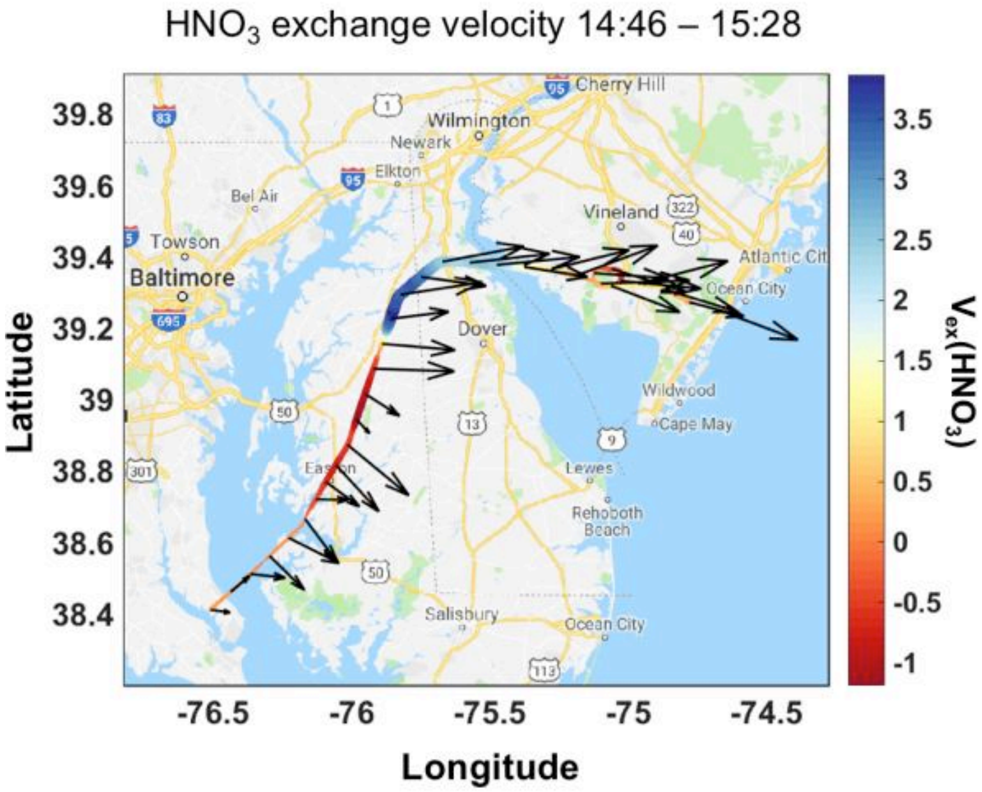

Figure 3.3 Spatial distribution of HNO_3 exchange velocity in RF 1. The black arrows indicate wind direction at the measurement points, with its size proportional to wind speed.

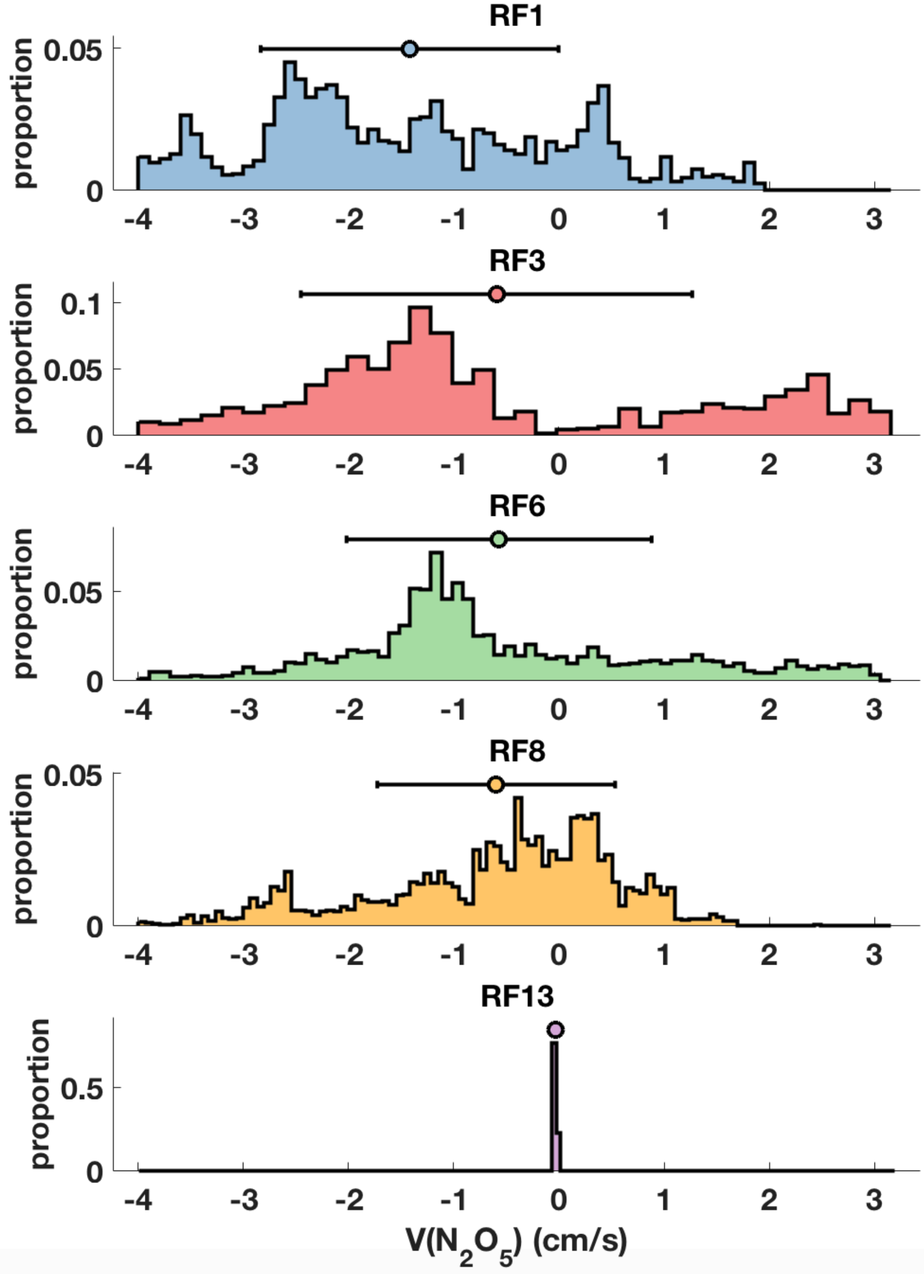

Figure 3.4. Histogram of wavelet-derived N_2O_5 exchange velocity frequency encountered in research flights over ocean surface. Horizontal error bar (mean ± standard deviation) is enclosed for each flight.

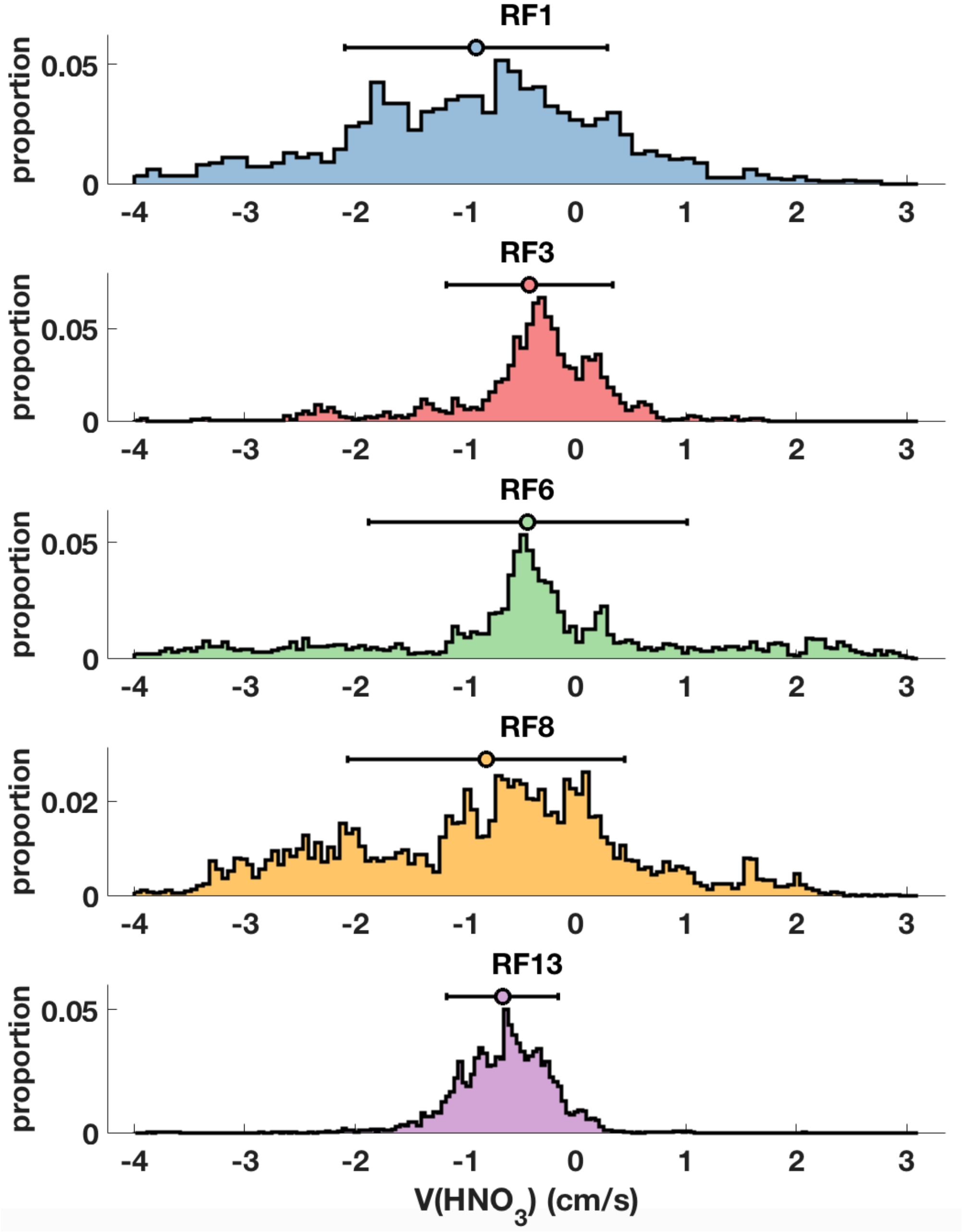

Figure 3.5 Histogram of wavelet-derived HNO_3 exchange velocity frequency encountered in research flights over ocean surface. Horizontal error bar (mean ± standard deviation) is enclosed for each flight.

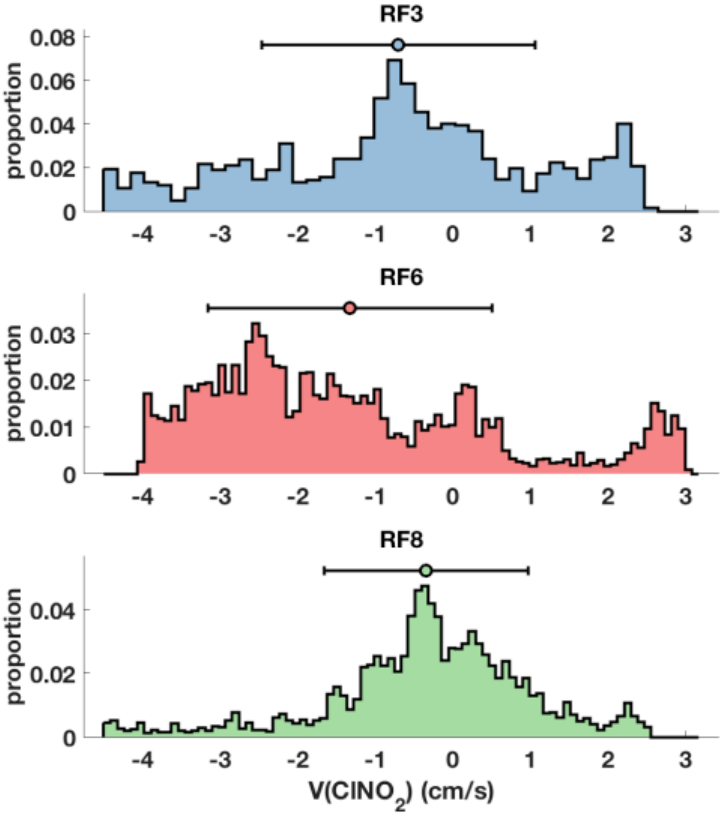

Figure 3.6 Histogram of wavelet-derived $ClNO_2$ exchange velocity frequency encountered in research flights over ocean surface. Horizontal error bar (mean ± standard deviation) is enclosed for each flight.

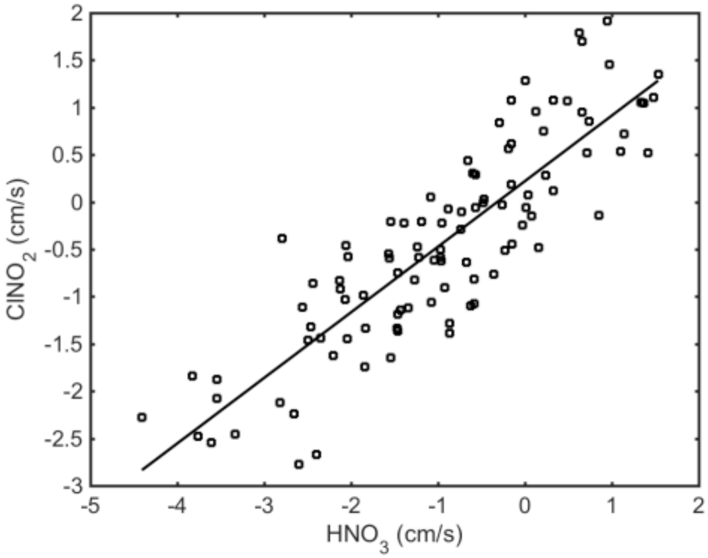

Figure 3.7. Correlation between wavelet-derived exchange velocity of HNO_3 and $ClNO_2$ in RF 8.

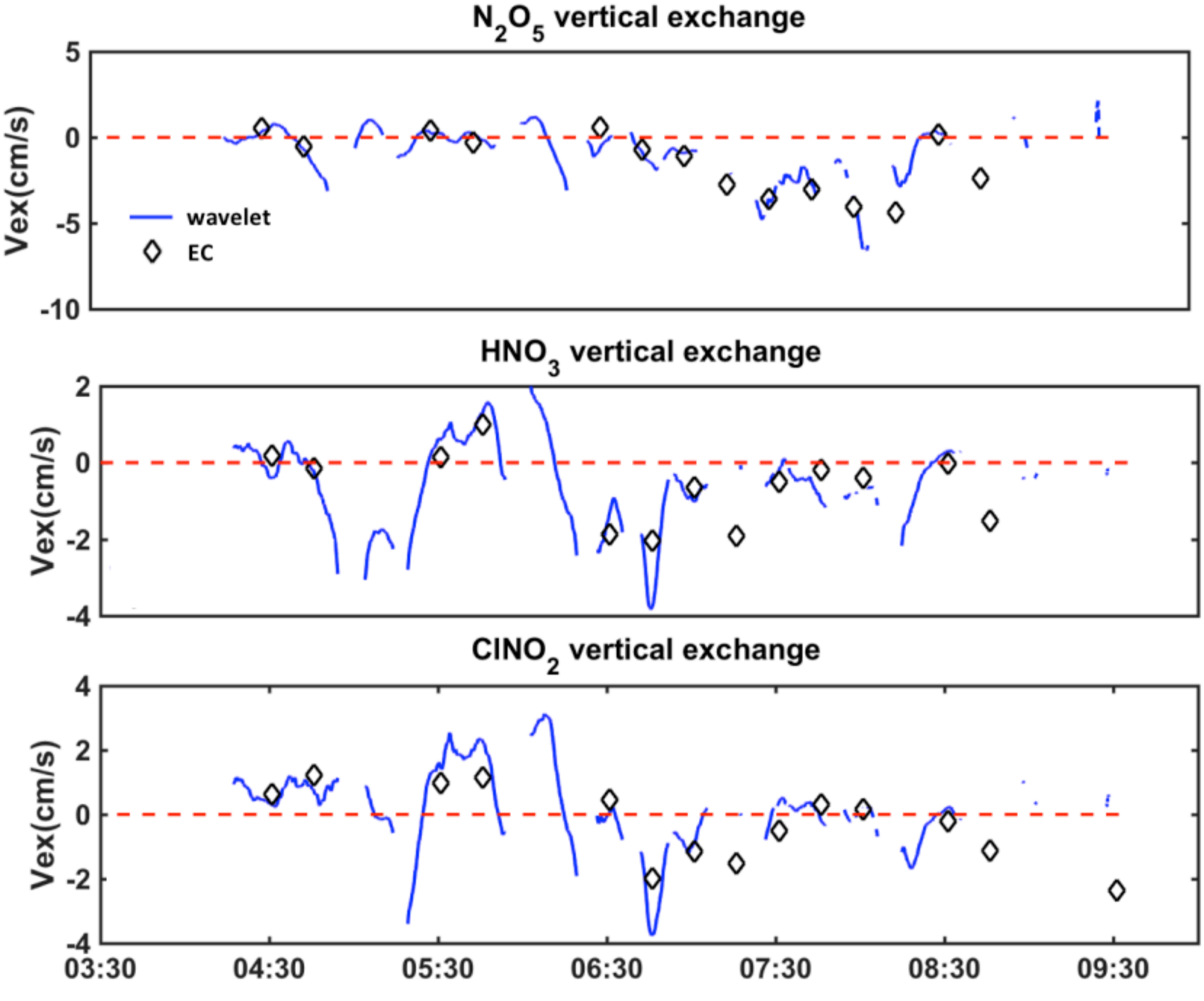

Figure 3.8. Exchange velocity derived by wavelet method (blue trace) and eddy covariance (black diamond, 15-min interval average) in RF 8.

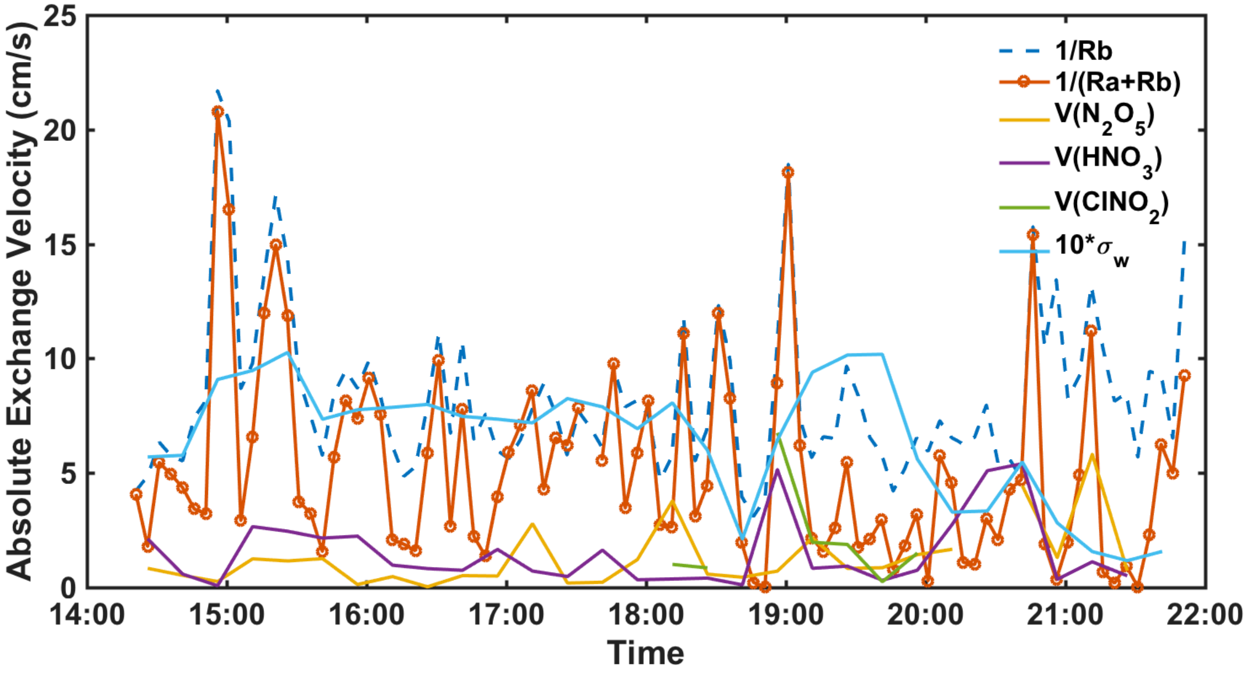

Figure 3.9. Time series of laminar layer conductance (1/Rb, blue dashed line), aerodynamic and laminar layer conductance (1/(Ra+Rb), orange dotted line), absolute exchange velocity for N_2O_5 (yellow), HNO_3 (purple), and $ClNO_2$ (green), and σ_w (10 times for better visualization, blue solid line) in RF 1. σ_w is the standard deviation of vertical wind speed and is a marker for turbulence.

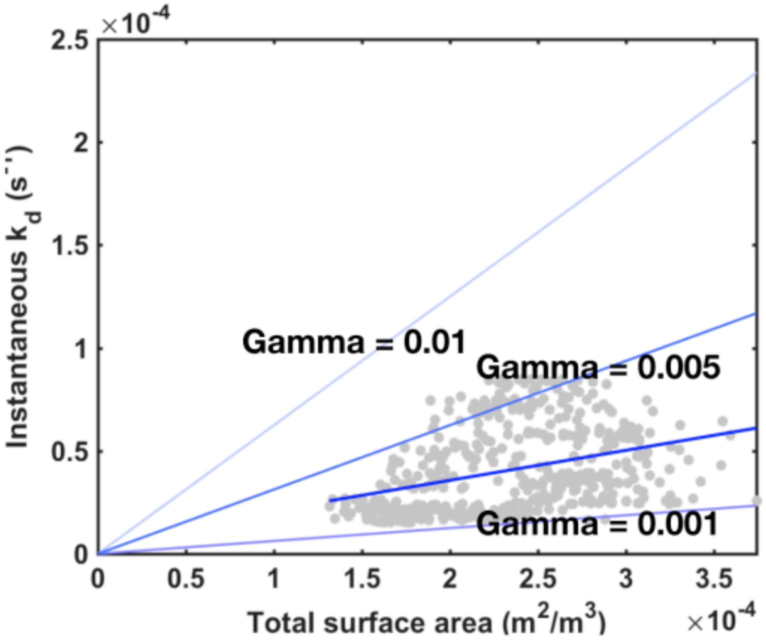

Figure 3.10. Instantaneous N_2O_5 deposition loss rates derived from wavelet exchange velocities of N_2O_5 (gray dots) as a function of measured total aerosol surface area. A linear fit is applied and shown in blue. Auxiliary lines for different gamma values are also plotted in convenience of comparison.

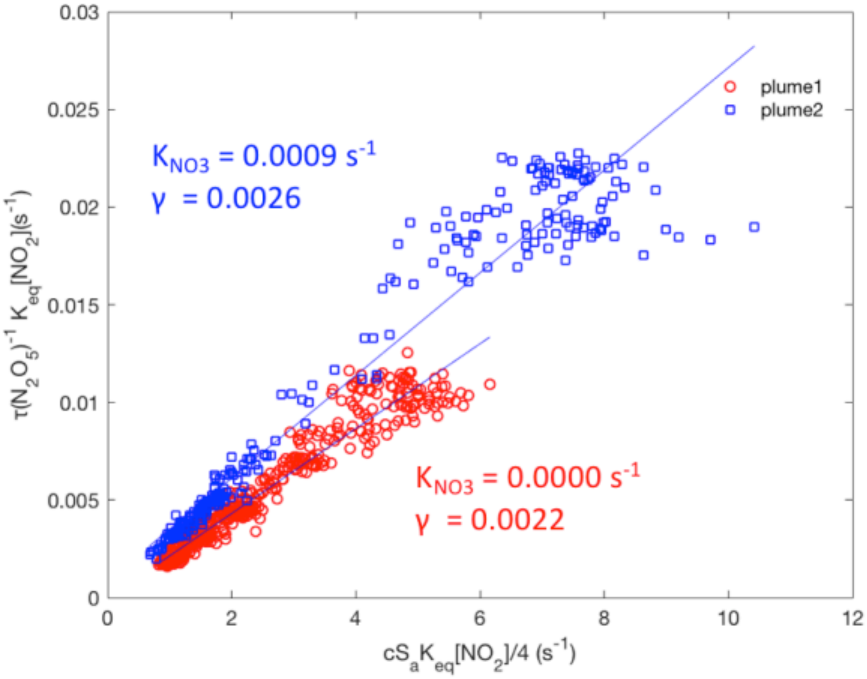

Figure 3.11. Correlation plot to determine N_2O_5 uptake coefficient in plume 1 and plume 2 in RF 8.

Chapter 4: Odd oxygen budget constraint

At night, NO_2 consumes O_3 and gives rise to a chain of oxidation products including NO_3 and N_2O_5. N_2O_5 could take part in heterogeneous reactions and form other reactive nitrogen species. This way, as NO_2 and O_3 reacted more time, they were stored in further oxidized species. If we group all these species into a chemical family, i.e. odd oxygen family, the interconversion cycles among these species could be eliminated. The total odd oxygen budget analysis is useful for keeping track of rapid chemical cycling that takes place between O_3 and other members of the odd-oxygen family without accounting for those individual reactions (Brown et al., 2006a). And as a result, the sum of these involved species multiplied by their respective stoichiometric coefficients should be conserved during the night if we ignore deposition and make some reasonable assumptions which are well-satisfied in our case (eg. NO_2 and O_3 uptake to aerosol is negligible; reactions with VOCs or DMS are negligible). We define the total odd oxygen species (Ox) as Eq. 6 below:

$$\text{(Eq. 6) } Ox = O_3 + NO_2 + 2NO_3 + 3N_2O_5 + \frac{3-\phi}{2-\phi} \bullet (HNO_3 + pNO_3^-) + ClNO_2$$

where the stoichiometric constants stand for the number of NO_2 and O_3 stored in each molecule, and φ is $ClNO_2$ yield from N_2O_5 heterogeneous uptake. The coefficient for total nitrate (sum of HNO_3 and pNO_3^-) is yield-dependent —1.5 for $\phi = 0$, and 2 for $\phi = 1$. Here, we used φ specific for the plume 1 in RF 8 in determining the coefficient ($\phi = 0.48$), as suggested in Fig. 4.1. The relevant transformation processes were illustrated in Figure 4.2. Dry deposition and heterogeneous processing resumes as plumes are transported downwind, but this incorporation saves us from complexity of considering the continuous acting physicochemical transformations in budget analysis. Therefore, in this study, the time rate of change of Ox is only affected by deposition and emissions if we assume that other pathways of Ox loss (eg. by the formation of organic nitrate) are minor and no repetitive measurements occurred. These situations have consequences for the ozone consumption during the night and therefore for the O_3 available the next day.

Several studies have illustrated that dry deposition plays an important role in the behavior of total Ox change. The modelling studies by Geyer and Stutz (2004) and many others suggested that the depositional term was in the same order of magnitude as the average nighttime Ox (O_3+NO_2+3N_2O_5) loss rate in urban scenarios, although their study might have underestimated the contribution of dry deposition without considering the heterogeneous reactions of N_2O_5. Few studies have quantified the vertical exchange of Ox species (especially more oxidized ones) and their impacts on Ox budget due to lack of accurate high-frequency instrumentations. Brown et al. (2007) measured high-resolution vertical profiles of NO_3 and N_2O_5 in the lowest 300 m of the NBL, but the lack of ancillary data prevented them from estimating Ox dynamics. In this study, we are enabled to carry out high resolution observations of a comprehensive suite of Ox species with HRToF-CIMS. In the following section, we dissect the factors that modulate Ox dynamics and the implication for constraining deposition velocities.

4.1 Ox dynamics and implications for Vex

Past field investigations have not explored the influence of reactive nitrogen deposition loss on Ox budget closure. Our direct measurements of Ox species above the ocean surface provided a unique opportunity to assess all of the dynamical components of the Ox budget in this coastal environment. In Fig. 4.3, we plotted the stacked time series of mixing ratios of Ox species. Considering the magnitude of the uncertainty, the change in total Ox mixing ratio in the plume is small, despite the regionally different meteorology and chemical conditions within the plume.

Nocturnal O_3 loss can be rationalized with active follow-up chemical transforms. The result also suggests that N_2O_5, HNO_3 and $ClNO_2$ has a non-negligible contribution to Ox in winter NBL. With the incorporation of dry deposition, the total undamped Ox mixing ratio is expected to remain constant within sampling error bound. That is, the slope of O_3 against the sum of other Ox species and deposition loss should be close to -1. By tuning the "lumped" exchange velocity suite for the Nr species, we could get a sense of how the addition of deposition influences the Ox budget. And ideally, we could close the Ox budget taking into account all the processes. The uncertainty is calculated as the quadrature sum of the measurement uncertainty for each Ox species involved. With an uncertainty range of 43% derived from the summer quadrature of instrument uncertainties involved, the slope of O_3 concentration against the sum of all other Ox components and deposition should be within the range of 0.57 – 1.43 with the ideal condition being close to unity. O_3 and NO_2 depositions are not included here assuming that was balanced by emissions. We adopted different values of Nr depositional rate, and see how the O_3-(ΣOx-O_3+deposition) slope changes and whether the slopes still fall within the range, as Fig. 4.4 shows. From this constraint, we could retrieve the upper limit average nighttime deposition velocity for Nr since sunset. Our wavelet-derived deposition velocities reside within the possible range, adding confidence to the analysis above.

4.2 Ox budget revisited with depositional correction

With a measurement of total reactive nitrogen and a quantification of their dry deposition rates, the relative contributions to odd oxygen loss with time in the boundary layer could be determined. The deposition rate coefficient ($K_{dep} = \frac{V_{dep}}{h}$ $in\ E5$) was calculated from the exchange velocity of N_2O_5 via wavelet measurements, and WINTER boundary layer heights over the ocean determined from the vertical profiles of potential temperature, as elaborated previously in section 3.2.1. Based on the flight-average K_{dep}, we could calculate the fractional loss of Nr with time assuming exponential decay and apply that to rescale the Nr mixing ratios to get the total Ox concentration without deposition. Nr deposition results in a large nocturnal loss: nearly 80% of HNO_3 is removed, and over 60% of N_2O_5 and over 50% of $ClNO_2$ is lost via deposition in a whole night. This significantly affects the NOx availability and O_3 production in the morning.

A caveat in closing Ox budget with vertical transport is that depositional losses of key nocturnal Ox species were not observed to be consistently as rapid within the marine boundary layer as assumed in this analysis, and the average value derived from our instantaneous exchange velocity measurements may not apply for plume conditions. That is, the N_2O_5 deposition velocity is variable and might be dependent on locations and chemistry regionally. A further uncertainty in this treatment is that HNO_3 might have variable chemical histories from multiple sources regions of different ages and initial conditions. This could potentially result in variable residence time and fractional loss. We will discuss this in the following section.

4.3 Figures

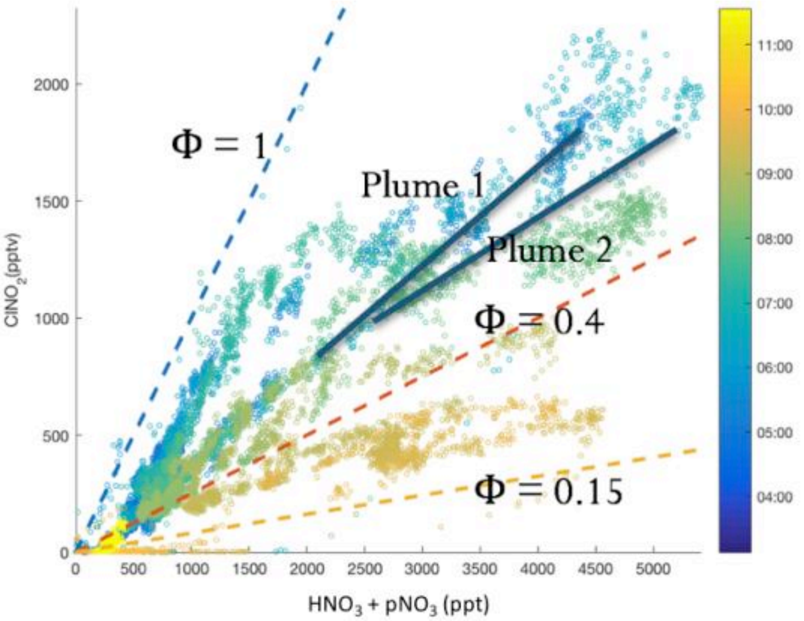

Figure 4.1. Scatter plot between $ClNO_2$ and total nitrate colored by time of day in RF 8. Linear fits are applied for plume 1 and plume 2. Auxiliary lines indicating different yields are also plotted.

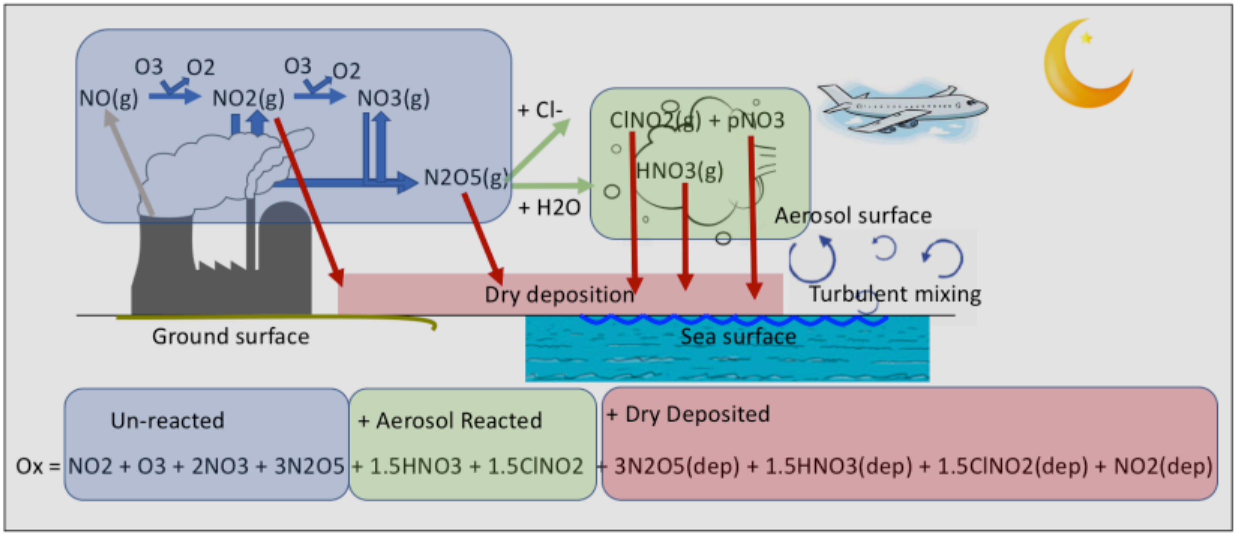

Figure 4.2. A schematic for nocturnal reactive nitrogen chemistry and odd oxygen budget.

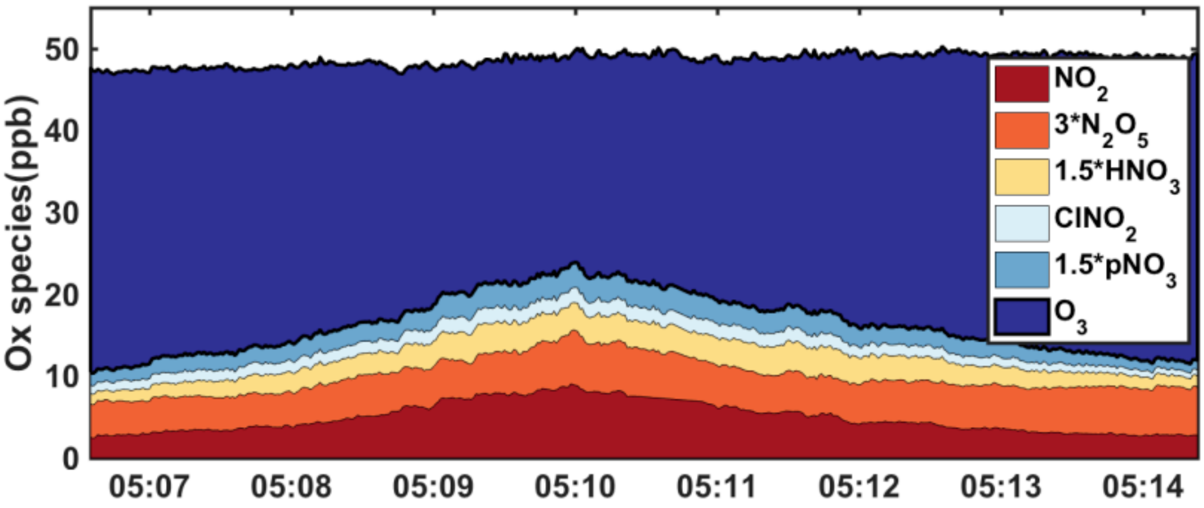

Figure 4.3. Stack time series of reactive nitrogen mixing ratios (multiplied by corresponding stoichiometric coefficients) for plume 1 in RF 8.

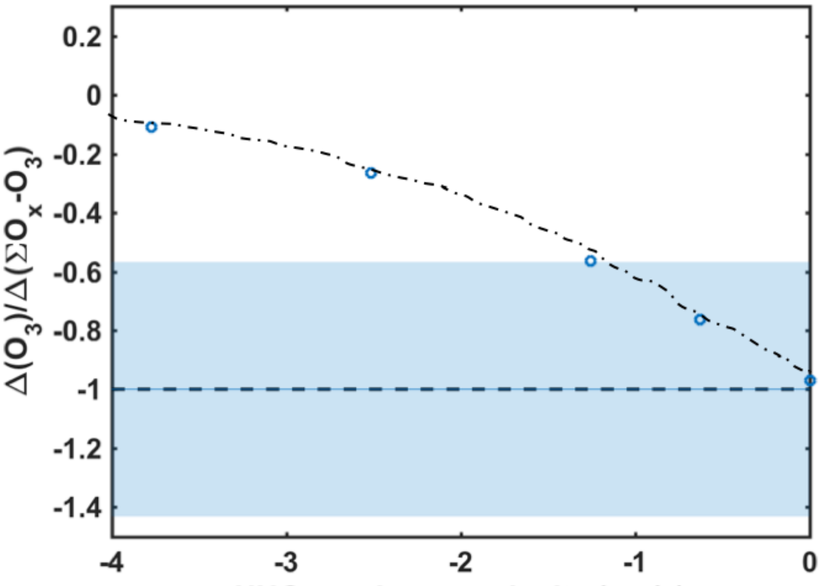

Figure 4.4. Ox budget constraint to exchange velocities: the variation of slope of Ox summation except for O_3 versus O_3 with Nr exchange velocities. The blue shading is the uncertainty range, and the exchange velocities fell in this range is valid.

Chapter 5: Simple box modelling of reactive nitrogen dynamics

5.1 HNO_3 source region and production

One important problem in Ox budget analysis is that HNO_3 may not be conserved. If an air mass were over water the entire night (~10 h), this would lead to a nearly 90% loss of HNO_3 as shown in Fig. 4.5, assuming marine boundary layer depth of 500–700 m. However, if the air masses are transported to the marine area in a land breeze after sunset, then HNO_3 underwent deposition from the air mass over land and thus the loss correction to surface by deposition could be different due to the different surface characteristics. Also, some of the HNO_3 may be produced from reaction between NO_2 and OH during the day and should be exempted from the nocturnal Ox budget analysis. All these factors complicate the Ox dynamics.

To study the origin of air masses sampled in the plume, backward dispersion calculations for 24 h prior to the sampling period using the Lagrangian Particle Dispersion Model FLEXPART (LPDM, Version 9.02, Stohl et al., 2005) as shown in Fig. 5.1. FLEXPART calculates the trajectories of an ensemble of air parcels (called particles) taking account of transport by mean flow, turbulence and sub-grid convection. Colleagues generated the 24-hour retroplumes for plume 1 observed in RF 8, and we use them here to show the column residence time of HNO_3 over water and to determine where the sampled air masses were potentially exposed to emissions. The retroplume analysis suggests that the observed plume originated from land, but is most likely to be reasonably homogeneous with parcels having similar histories that may have mixed prior to the observation. It shows that the air mass spent over 14 hours over water, which means that the entirety of its path was above ocean surface after sunset despite a land origin, suggesting a relatively uniform deposition environment. Meanwhile, as shown in Fig.

5.2, there is a good linearity between HNO_3 and particulate nitrate, which further implies a homogeneous environment. These conditions provide a near ideal case study for investigating the impacts of dry deposition on the chemical evolution of Nr.

5.2 Simple box modelling of reactive nitrogen dynamics

Although the Ox budget provides a convenient way to verify the impact of deposition, the dominantly large contributions of NO_2 and O_3 might make it difficult to accurately constrain the deposition rates of trace reactive nitrogen species that we are interested in. Therefore, we employed a zero-dimensional box model fitted with chemical mechanisms (R1)–(R5) including deposition to explore the evolution of Nr as a complemental study. This box model is used to characterize nocturnal reactive nitrogen chemistry with an emphasis on the depositional loss effect. The main assumptions of this approach are that air masses with similar histories were sampled throughout the night and the air mass underwent only chemical transformation without dilution or mixing during this transport. These simulations only serve as back-of-the-envelope type estimates of major processes as an accurate description of the nocturnal boundary layer chemistry would require the input of altitude-resolved information. A series of additional sensitivity runs were conducted in which we altered the deposition velocity and mixed layer depth in order to account for the uncertainty and evaluate the importance of different factors.

(R1) $NO_2 + O_3 \longrightarrow NO_3 + O_2$

(R2) $NO_3 + NO_2 + M \rightleftharpoons N_2O_5$

(R3) $N_2O_5 + H_2O(het) \longrightarrow 2HNO_3$

(R4) $N_2O_5 + Cl^-(het) \longrightarrow ClNO_2 + NO_3^-$

(R5) $N_2O_5, HNO_3, ClNO_2 \longrightarrow$ deposition

The initial time zero is set at local sunset (6 pm) and continues for 16 hours. Titration with NO occurs rapidly reducing O_3 mixing ratios at the plume center, so we initiated the box model with the maximum nocturnal NO_2 and O_3 mixing ratios to compensate for this. The simulation includes time development of selected trace gas observations—such as O_3, NO_2, and Nr—and meteorology—temperature and boundary layer height —as input. The box model boundary layer height, or effectively a mixing depth, controlled the range over which emissions are mixed into the model, as well as the rate of sinks via deposition. We fix it to 500 m as concluded from inspecting the potential temperature vertical profiles for RF 8. In the following sections, we will examine the simulated mixing ratios in comparison with the measurements in the plume intercept.

5.2.1 Without deposition

In modelling the Nr concentrations, the first step is to hold γ constant at an arbitrary initial value (eg. 0.01) and iteratively adjusts the initial concentrations of NO_2 and O_3 until the final simulated mixing ratios are within 5% of the measurements. The second step holds these derived-initial concentrations constant while iteratively adjusting γ until the simulated N_2O_5 is within 5% of the observed mixing ratio. Steps 1 and 2 are repeated until NO_2, O_3, and N_2O_5 simultaneously meet their respective fit criteria. The third step holds all derived parameters constant while iteratively adjusting ϕ until the final simulated mixing ratio of $ClNO_2$ is within 5% of observations. An uptake coefficient of $\gamma = 0.0058$ and yield of $\phi(ClNO_2) = 0.45$ would bring the modelled $[N_2O_5]$ and $[ClNO_2]$ into agreement with observation, as shown in Fig. 5.3 (left). It turns out that all the nitrogen species except for total nitrate (HNO_3 + pNO_3) could reasonably match the measurements, while the total nitrate levels were far below predictions from the box model by over 2 ppb, which might result from neglecting deposition and super-micron nitrate. In the following sections, we add deposition to the box model to investigate their influence on subsequent processes.

5.2.2 With Nr deposition

Here we turn on pseudo-first order depositional loss for all three reactive nitrogen species using the median exchange velocities derived in section 3.2 – -0.78 cm • s^{-1}, -0.68 cm • s^{-1}, -0.73 cm • s^{-1} for N_2O_5, HNO_3 and $ClNO_2$, respectively. The depositional loss of particle-phase nitrate is generally on the order of several days, thus we only consider the gas-phase depositional loss (HNO_3) with its contribution to total nitrate. Using the parameters determined in the preceding sections as well as the deposition velocities derived from wavelet analysis, we compared the model and observation mixing ratios in the plume center.

As shown in Fig. 5.3 (right), inclusion of deposition resolves the discrepancy between observation and simulations for total nitrate by invoking an uptake coefficient of $\gamma(N_2O_5) = 0.0048$ and yield of $\phi(ClNO_2) = 0.73$. Our observation-based model fully reconciles measured and predicted Nr in the marine boundary layer after accounting for the dry deposition losses. McDuffie et al. (2018) conducted an iterative box modeling analysis constrained with WINTER observations of NO_2, O_3, N_2O_5, and $ClNO_2$ to infer $\gamma(N_2O_5)$, and found $\gamma(N_2O_5) = 0.0045 \pm 0.0013$ for this flight (RF 8), which is comparable to what we calculate with our simplistic box model.

Considering that we have already compensated for depositional loss embodied in the initial NO_2 and O_3 mixing ratio, we exclude NO_2 and O_3 deposition and dispersion in the box model. Although this analysis focused on comparisons only within a short time period, the chemistry characterized is in agreement with previous modeling work and lends confidence to the state of knowledge regarding reactive nitrogen chemistry, and the implicit deposition losses (Jaeglé et al., 2018). The agreement between box model predictions and observations illustrates that our methods of treating the reactive nitrogen deposition in the wavelet analysis and in the box model are self-consistent.

One thing to note is that in the treatment above, we used HR-AMS nitrate only since UNH nitrate lost the non-refractory ammonium nitrate due to partial evaporation and decomposition, and its temporal resolution is not high enough. While AMS lost coarse mode super-micron nitrate like sodium nitrate, it only insignificantly affects the outcome due to the low contribution of these coarser particles to N_2O_5 uptake. Both approaches encounter a sampling bias. As shown in Fig. 5.4, there is quite good agreement between UNH nitrate and AMS nitrate until we get into the plumes which had elevated urban outflow that aged overnight, possibly owing to the higher temperature and humidity. When the total nitrate level is low, and/or particle phase NH_4NO_3 is a small fraction of the total nitrate, even with warmer cabin temperatures compared to ambient temperatures, the bias between the filters and HR-AMS NO_3^- will be low. This case is not representative of the conditions experienced during most of the ambient conditions as we encountered high concentrations of particulate nitrate in RF 8.

5.2.3 Sensitivity analysis

The modeled mixing ratios are subject to uncertainties in deposition velocities, so we performed sensitivity analyses to estimate their effect on the simulations. The base case is to use the parameters (γ and ϕ) determined previously, and ignore any deposition. We tested the sensitivity by doubling or halving the Nr deposition velocity (or deposition loss rate) simultaneously and compare how it changes the mixing ratio in the plume peak. Results are shown in Fig. 5.5. The data shows -19.3% and 12.7% changes on average for concentrations of the three reactive nitrogen species, respectively. Note that a change in the estimation of boundary layer height would directly impact all depositional loss rates simultaneously, and resultantly alter the fraction of chemical removal that is due to surface deposition, as it controls the "volume of the box" within which mixing and dispersion of trace gases and aerosol particles take place. This effect is essentially equivalent to scaling the Nr deposition velocities and thus not discussed separately.

5.4 Figures

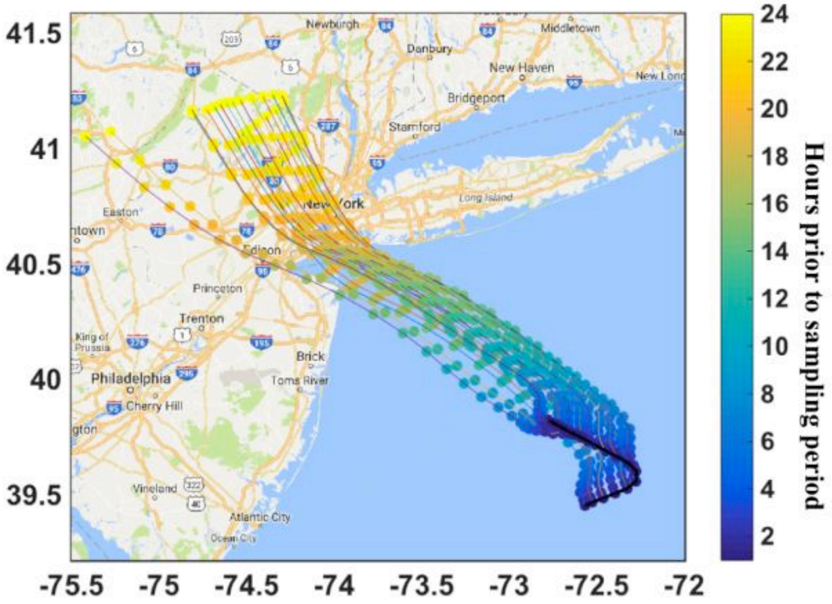

Figure 5.1. FLEXPART backward air trajectories calculated for 24 h prior to sampling for plume 1 in RF 8. The black curve stands for flight track.

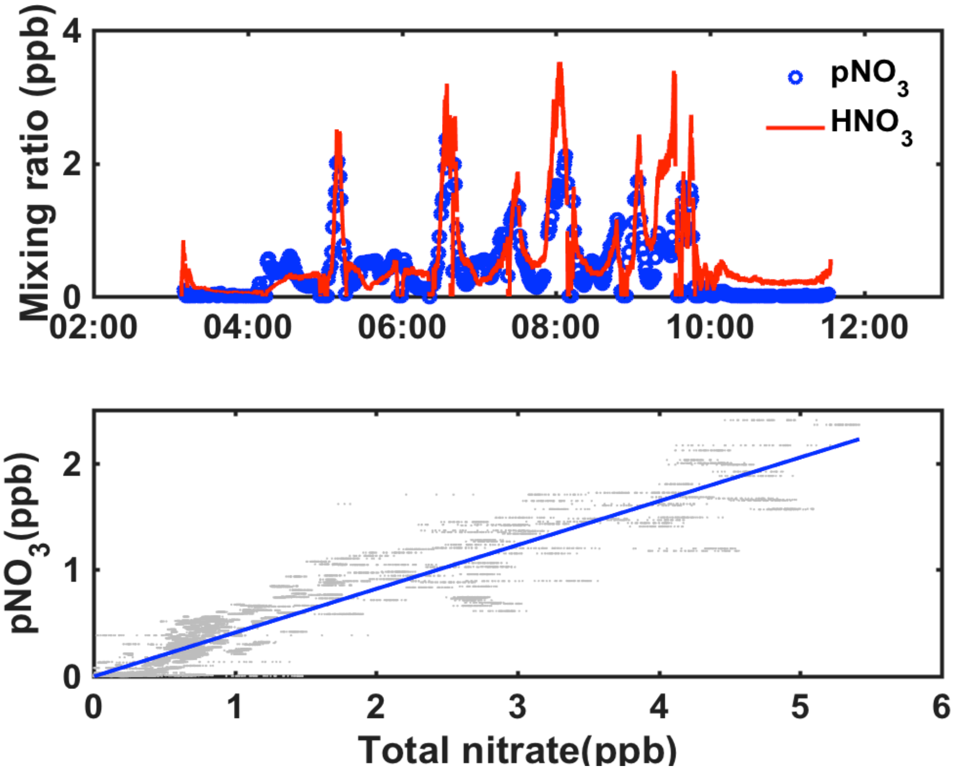

Figure 5.2 Time series (upper panel) and correlation plot (lower panel) of particulate nitrate and nitric acid in RF 8.

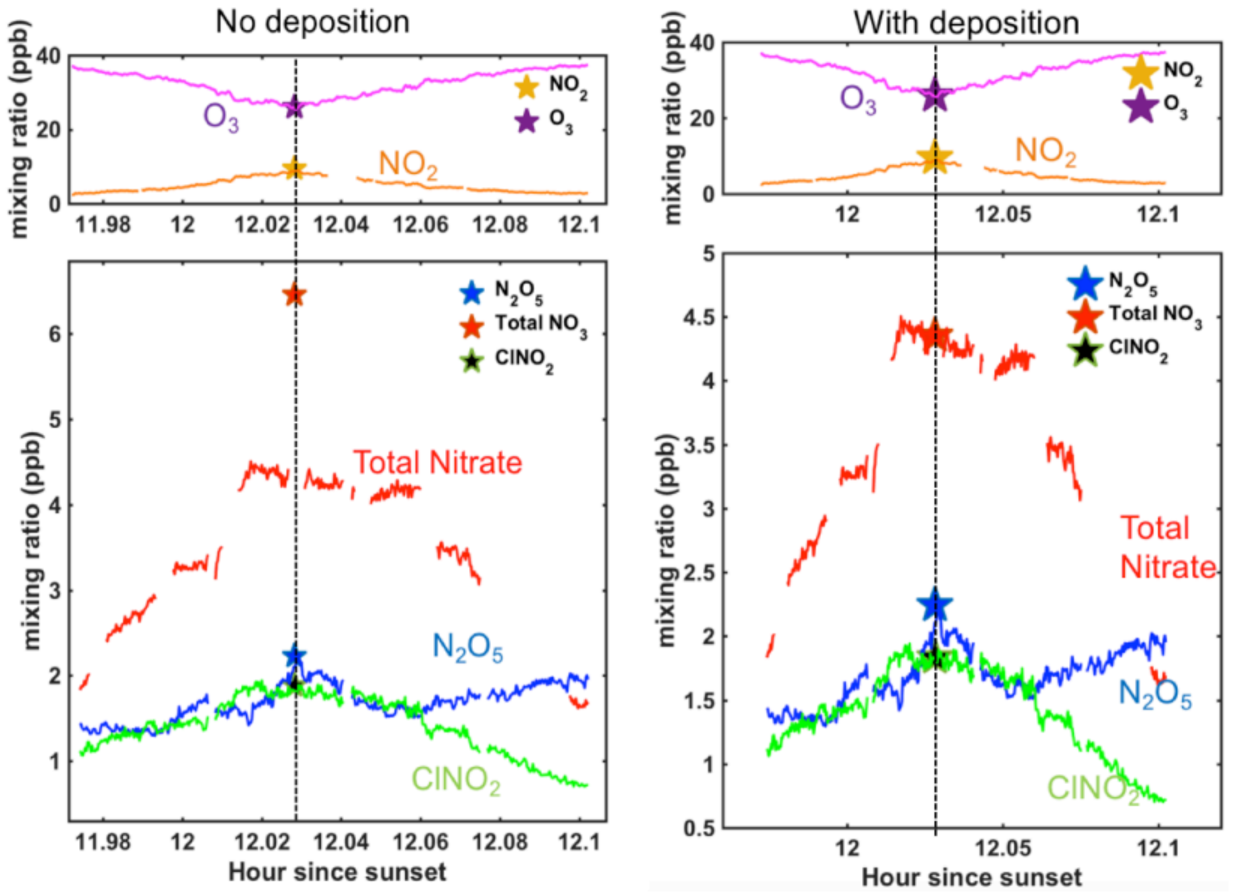

Figure 5.3. Observation-based box model prediction (denoted by stars) and measurement of trace gas concentrations (curves) for plume 1 in RF 8. (left) no deposition is imposed; (right) Nr deposition is imposed using the wavelet derived V_d results.

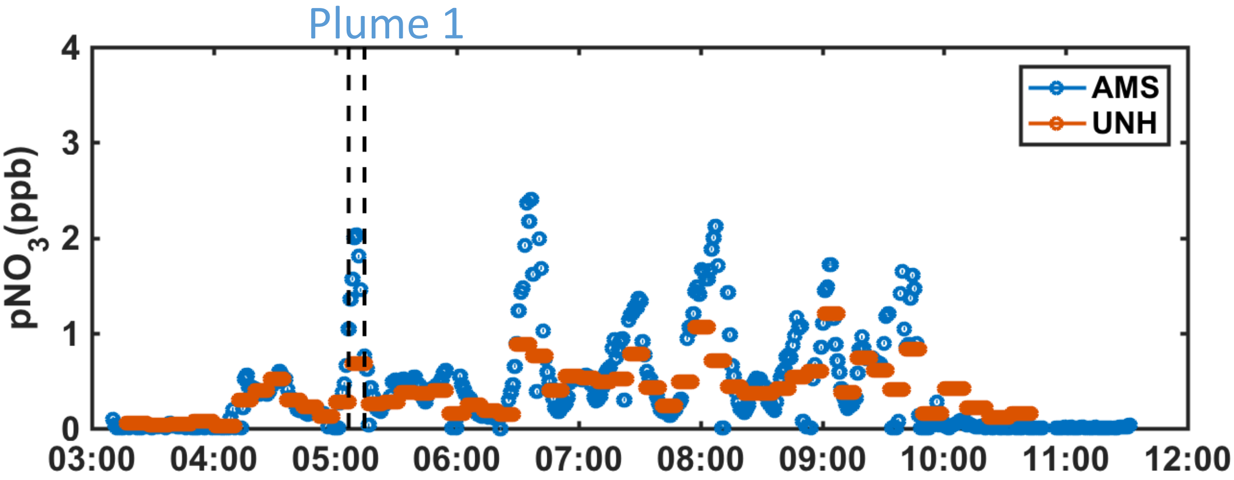

Figure. 5.4 Times series of particulate nitrate measured by aerosol mass spectrometer (AMS) and UNH in RF 8. Plume 1 period is labelled and partitioned with black dashed lines.

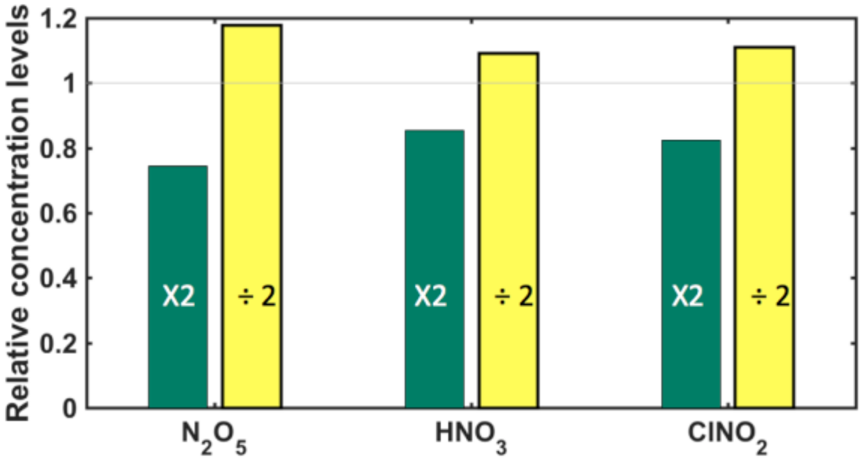

Figure. 5.5 Sensitivity analysis of box model predicted Nr concentrations relative to observation by doubling or halving the wavelet-derived Nr deposition velocity simultaneously.

Chapter 6: Conclusions and Discussions

The results presented in this paper highlight the viability of high-frequency measurements of reactive nitrogen compounds by HRToF-CIMS in tandem with micrometeorological techniques for direct, in situ study of eddy fluxes over ocean. As the critical input parameter for atmospheric models, deposition velocities have not been quantitatively studied enough. The ability to calculate fluxes at high temporal/spatial resolution with Continuous Wavelet Transform (CWT) method provides a good source to compare measured deposition loss rate with simulated total loss rate from box models. The good agreement between airborne eddy covariance flux measurements and wavelet flux highlights the utility of wavelet analysis and related time series analysis tools to advance our mechanistic understanding in exchange of Nr species across heterogeneous terrains. The odd oxygen budget closure within measurement uncertainty placed constraints on the possible range of the deposition velocity of Nr, and testified that our eddy covariance results were reasonable. A simple box model was carried out to make some semi-quantitative statements about the exchange rates for Nr. Sensitivity analysis shows that N_2O_5 hydrolysis strongly regulates O_3 and NOx burdens, and incorporating dry deposition in the box model could significantly shift the derived uptake coefficient and $ClNO_2$ yield. Thus, an accurate prediction of the influence of N_2O_5 uptake on NOx and oxidants remains a complicated problem. We also investigated the role of ocean surfaces relative to aerosol particles in the uptake of N_2O_5, and it turns out that the deposition accounted for roughly 1/6 of the total N_2O_5 loss. These results are essential for constraining deposition in regional and global models where hydrolysis of N_2O_5 is thought to be a dominant pathway for the loss of reactive nitrogen. It still appears to be very difficult to obtain direct observational evidence to discern between different depositional mechanisms. Therefore, more observations from different environments are required to enable models to better predict the extent of Nr deposition and the variability of these nocturnal processes. Further work is needed to ascertain the branching between N_2O_5 heterogeneous pathways and its importance for nitrogen cycle as well as Ox budget in the troposphere with larger observation datasets.

One thing to mention is that our current understanding comes from a chemical system with relatively low turbulence at night and warrants more speculations. The unfavorable observation conditions and the difficulties in modelling the entire vertical extent of the nocturnal atmosphere have inhibited a better understanding of the impact of reactive nitrogen exchange. The intrinsic stagnant feature of the winter nighttime boundary layer limits the perfect mixing requirement of the eddy covariance computation. However, with relatively high wind speeds and low atmospheric stability over sea surface (see our clarifications in Section 2.4), our results still provide a sufficiently robust reference for quantifying Nr exchange velocities.

Bibliography

Apodaca, R. L., Huff, D. M., & Simpson, W. R. (2008). The role of ice in N2O5 heterogeneous hydrolysis at high latitudes. *Atmospheric Chemistry and Physics*, *8*(24), 7451-7463.

Ammann, C., Wolff, V., Marx, O., Brümmer, C., & Neftel, A. (2012). Measuring the biosphere-atmosphere exchange of total reactive nitrogen by eddy covariance. *Biogeosciences*, *9*(11), 4247-4261.

Aldener, M., Brown, S. S., Stark, H., Williams, E. J., Lerner, B. M., Kuster, W. C., ... & Ravishankara, A. R. (2006). Reactivity and loss mechanisms of NO3 and N2O5 in a polluted marine environment: Results from in situ measurements during New England Air Quality Study 2002. *Journal of Geophysical Research: Atmospheres*, *111*(D23).

Baldocchi, D. (2014). Measuring fluxes of trace gases and energy between ecosystems and the atmosphere–the state and future of the eddy covariance method. *Global change biology*, *20*(12), 3600-3609.

Behnke, W., George, C., Scheer, V., & Zetzsch, C. (1997). Production and decay of ClNO2 from the reaction of gaseous N2O5 with NaCl solution: Bulk and aerosol experiments. *Journal of Geophysical Research: Atmospheres*, *102*(D3), 3795-3804.

Brasseur, G. P., Hauglustaine, D. A., Walters, S., Rasch, P. J., Müller, J. F., Granier, C., & Tie, X. X. (1998). MOZART, a global chemical transport model for ozone and related chemical tracers: 1. Model description. *Journal of Geophysical Research: Atmospheres*, *103*(D21), 28265-28289.

Bertram, T. H., Thornton, J. A., Riedel, T. P., Middlebrook, A. M., Bahreini, R., Bates, T. S., ... & Coffman, D. J. (2009). Direct observations of N2O5 reactivity on ambient aerosol particles. *Geophysical Research Letters*, *36*(19).

Brown, S. S., Stark, H., & Ravishankara, A. R. (2003). Applicability of the steady state approximation to the interpretation of atmospheric observations of NO3 and N2O5. *Journal of Geophysical Research: Atmospheres*, *108*(D17).

Brown, S. S., Neuman, J. A., Ryerson, T. B., Trainer, M., Dubé, W. P., Holloway, J. S., ... & Matthew, B. (2006). Nocturnal odd-oxygen budget and its implications for ozone loss in the lower troposphere. *Geophysical Research Letters*, *33*(8).

Brown, S. S., Dubé, W. P., Osthoff, H. D., Stutz, J., Ryerson, T. B., Wollny, A. G., ... & Neuman, J. A. (2007). Vertical profiles in NO3 and N2O5 measured from an aircraft: Results from the NOAA P-3 and surface platforms during the New England Air Quality Study 2004. *Journal of Geophysical Research: Atmospheres*, *112*(D22).

Baldocchi, D. D., Hincks, B. B., & Meyers, T. P. (1988). Measuring biosphere-atmosphere exchanges of biologically related gases with micrometeorological methods. *Ecology*, *69*(5), 1331-1340.

Farmer, D. K., Wooldridge, P. J., & Cohen, R. C. (2006). Application of thermal-dissociation laser induced fluorescence (TD-LIF) to measurement of HNO 3, Σalkyl nitrates, Σperoxy nitrates, and NO 2 fluxes using eddy covariance. *Atmospheric Chemistry and Physics*, *6*(11), 3471-3486.

Farmer, D. K., & Cohen, R. C. (2008). Observations of HNO 3, ΣAN, ΣPN and NO 2 fluxes: Evidence for rapid HO x chemistry within a pine forest canopy. *Atmospheric Chemistry and Physics*, *8*(14), 3899-3917.

Geddes, J. A., & Murphy, J. G. (2014). Observations of reactive nitrogen oxide fluxes by eddy covariance above two midlatitude North American mixed hardwood forests. *Atmospheric Chemistry and Physics*, *14*(6), 2939-2957.

Huff, D. M., Joyce, P. L., Fochesatto, G. J., & Simpson, W. R. (2011). Deposition of dinitrogen pentoxide, N 2 O 5, to the snowpack at high latitudes. *Atmospheric Chemistry and Physics*, *11*(10), 4929-4938.

Heald, C. L., Collett Jr, J. L., Lee, T., Benedict, K. B., Schwandner, F. M., Li, Y., ... & Coheur, P. F. (2012). Atmospheric ammonia and particulate inorganic nitrogen over the United States. *Atmospheric Chemistry and Physics*, *12*(21), 10295-10312.

Jaeglé, L., Shah, V., Thornton, J. A., Lopez-Hilfiker, F. D., Lee, B. H., McDuffie, E. E., ... & Ebben, C. J. (2018). Nitrogen oxides emissions, chemistry, deposition, and export over the Northeast United States during the WINTER aircraft campaign. *Journal of Geophysical Research: Atmospheres*, *123*(21), 12-368.

Kaimal, J. C., Wyngaard, J. C. J., Izumi, Y., & Coté, O. R. (1972). Spectral characteristics of surface-layer turbulence. *Quarterly Journal of the Royal Meteorological Society*, *98*(417), 563-589.

Kim, M. J., Farmer, D. K., & Bertram, T. H. (2014). A controlling role for the air− sea interface in the chemical processing of reactive nitrogen in the coastal marine boundary layer. *Proceedings of the National Academy of Sciences*, *111*(11), 3943-3948.

Lenschow, D. H., & Raupach, M. R. (1991). The attenuation of fluctuations in scalar concentrations through sampling tubes. *Journal of Geophysical Research: Atmospheres*, *96*(D8), 15259-15268.

Lopez-Hilfiker, F. D., Constantin, K., Kercher, J. P., & Thornton, J. A. (2012). Temperature dependent halogen activation by N 2 O 5 reactions on halide-doped ice surfaces. *Atmospheric Chemistry and Physics*, *12*(11), 5237-5247.

Lee, B. H., Lopez-Hilfiker, F. D., Mohr, C., Kurtén, T., Worsnop, D. R., & Thornton, J. A. (2014). An iodide-adduct high-resolution time-of-flight chemical-ionization mass spectrometer: Application to atmospheric inorganic and organic compounds. *Environmental science & technology*, *48*(11), 6309-6317.

Liu, Y., San Liang, X., & Weisberg, R. H. (2007). Rectification of the bias in the wavelet power spectrum. *Journal of Atmospheric and Oceanic Technology*, *24*(12), 2093-2102.

Mentel, T. F., Sohn, M., & Wahner, A. (1999). Nitrate effect in the heterogeneous hydrolysis of dinitrogen pentoxide on aqueous aerosols. *Physical Chemistry Chemical Physics*, *1*(24), 5451-5457.

Moncrieff, J. B., Massheder, J. M., De Bruin, H., Elbers, J., Friborg, T., Heusinkveld, B., ... & Verhoef, A. (1997). A system to measure surface fluxes of momentum, sensible heat, water vapour and carbon dioxide. *Journal of Hydrology*, *188*, 589-611.

Munger, J. W., Jacob, D. J., Fan, S. M., Colman, A. S., & Dibb, J. E. (1999). Concentrations and snow-atmosphere fluxes of reactive nitrogen at Summit, Greenland. *Journal of Geophysical Research: Atmospheres*, *104*(D11), 13721-13734.

McDuffie, E. E., Fibiger, D. L., Dubé, W. P., Lopez-Hilfiker, F., Lee, B. H., Thornton, J. A., ... & Michael Reeves, J. (2018). Heterogeneous N2O5 uptake during winter: Aircraft measurements during the 2015 WINTER campaign and critical evaluation of current parameterizations. *Journal of Geophysical Research: Atmospheres*, *123*(8), 4345-4372.

Mauder, M., Oncley, S. P., Vogt, R., Weidinger, T., Ribeiro, L., Bernhofer, C., ... & Liu, H. (2007). The energy balance experiment EBEX-2000. Part II: Intercomparison of eddy-covariance sensors and post-field data processing methods. *Boundary-Layer Meteorology*, *123*(1), 29-54.

Meyers, T. P., Hicks, B. B., Hosker Jr, R. P., Womack, J. D., & Satterfield, L. C. (1991). Dry deposition inferential measurement techniques—II. Seasonal and annual deposition rates of sulfur and nitrate. *Atmospheric Environment. Part A. General Topics*, *25*(10), 2361-2370.

Neftel, A., Blatter, A., Hesterberg, R., & Staffelbach, T. (1996). Measurements of concentration gradients of HNO2 and HNO3 over a semi-natural ecosystem. *Atmospheric Environment*, *30*(17), 3017-3025.

Nemitz, E., Sutton, M. A., Wyers, G. P., & Jongejan, P. A. C. (2004). Gas-particle interactions above a Dutch heathland: I. Surface exchange fluxes of NH 3, SO2, HNO3 and HCl. *Atmospheric Chemistry and Physics*, *4*(4), 989-1005.

Nguyen, T. B., Crounse, J. D., Teng, A. P., Clair, J. M. S., Paulot, F., Wolfe, G. M., & Wennberg, P. O. (2015). Rapid deposition of oxidized biogenic compounds to a temperate forest. *Proceedings of the National Academy of Sciences*, *112*(5), E392-E401.

Nemitz, E., Sutton, M. A., Wyers, G. P., & Jongejan, P. A. C. (2004). Gas-particle interactions above a Dutch heathland: I. Surface exchange fluxes of NH 3, SO 2, HNO 3 and HCl. *Atmospheric Chemistry and Physics*, *4*(4), 989-1005.

Osthoff, H. D., Roberts, J. M., Ravishankara, A. R., Williams, E. J., Lerner, B. M., Sommariva, R., ... & Stark, H. (2008). High levels of nitryl chloride in the polluted subtropical marine boundary layer. *Nature Geoscience*, *1*(5), 324.

Phillips, G. J., Makkonen, U., Schuster, G., Sobanski, N., Hakola, H., & Crowley, J. N. (2013). The detection of nocturnal N2O5 as HNO3 by alkali-and aqueous-denuder techniques. *Atmospheric Measurement Techniques*, *6*(2), 231-237.

Phillips, G. J., Thieser, J., Tang, M., Sobanski, N., Schuster, G., Fachinger, J., ... & Crowley, J. N. (2016). *Estimating N2O5 uptake coefficients using ambient measurements of NO3, N2O5, ClNO2 and particle-phase nitrate*. Universitätsbibliothek Johann Christian Senckenberg.

Riemer, N., Vogel, H., Vogel, B., Schell, B., Ackermann, I., Kessler, C., & Hass, H. (2003). Impact of the heterogeneous hydrolysis of N2O5 on chemistry and nitrate aerosol formation in the lower troposphere under photosmog conditions. *Journal of Geophysical Research: Atmospheres*, *108*(D4).

Sutton, M. A., Howard, C. M., Erisman, J. W., Bealey, W. J., Billen, G., Bleeker, A., ... & Grizzetti, B. (2011). The challenge to integrate nitrogen science and policies: the European Nitrogen Assessment approach.

Stutz, J., Alicke, B., Ackermann, R., Geyer, A., White, A., & Williams, E. (2004). Vertical profiles of NO3, N2O5, O3, and NOx in the nocturnal boundary layer: 1. Observations during the Texas Air Quality Study 2000. *Journal of Geophysical Research: Atmospheres*, *109*(D12).

Stohl, A., Forster, C., Frank, A., Seibert, P., & Wotawa, G. (2005). The Lagrangian particle dispersion model FLEXPART version 6.2. *Atmospheric Chemistry and Physics*, *5*(9), 2461-2474.

Sifuzzaman, M., Islam, M. R., & Ali, M. Z. (2009). Application of wavelet transform and its advantages compared to Fourier transform.

Schobesberger, S., Lopez-Hilfiker, F. D., Taipale, D., Millet, D. B., D'Ambro, E. L., Rantala, P., ... & Boy, M. (2016). High upward fluxes of formic acid from a boreal forest canopy. *Geophysical Research Letters*, *43*(17), 9342-9351.

Smeets, C. J. P. P., Holzinger, R., Vigano, I., Goldstein, A. H., & Röckmann, T. (2009). Eddy covariance methane measurements at a Ponderosa pine plantation in California. *Atmospheric Chemistry and Physics*, *9*(21), 8365-8375.

Sander, R., & Crutzen, P. J. (1996). Model study indicating halogen activation and ozone destruction in polluted air masses transported to the sea. *Journal of Geophysical Research: Atmospheres*, *101*(D4), 9121-9138.

Strunin, M. A., Hiyama, T., Asanuma, J., & Ohata, T. (2004). Aircraft observations of the development of thermal internal boundary layers and scaling of the convective boundary layer over non-homogeneous land surfaces. *Boundary-layer meteorology*, *111*(3), 491-522.

Thornton, J. A., Kercher, J. P., Riedel, T. P., Wagner, N. L., Cozic, J., Holloway, J. S., ... & Alexander, B. (2010). A large atomic chlorine source inferred from mid-continental reactive nitrogen chemistry. *Nature*, *464*(7286), 271.

Thornton, J. A., & Abbatt, J. P. (2005). N2O5 reaction on submicron sea salt aerosol: Kinetics, products, and the effect of surface active organics. *The Journal of Physical Chemistry A*, *109*(44), 10004-10012.

Terradellas, E., Morales, G., Cuxart, J., & Yagüe, C. (2001). Wavelet methods: application to the study of the stable atmospheric boundary layer under non-stationary conditions. *Dynamics of Atmospheres and Oceans*, *34*(2-4), 225-244.

Torrence, C., & Compo, G. P. (1998). A practical guide to wavelet analysis. *Bulletin of the American Meteorological society*, *79*(1), 61-78.

Vickers, D., Göckede, M., & Law, B. (2010). Uncertainty estimates for 1-h averaged turbulence fluxes of carbon dioxide, latent heat and sensible heat. *Tellus B: Chemical and Physical Meteorology*, *62*(2), 87-99.

Webb, E. K., Pearman, G. I., & Leuning, R. (1980). Correction of flux measurements for density effects due to heat and water vapour transfer. *Quarterly Journal of the Royal Meteorological Society*, *106*(447), 85-100.

Wolfe, G. M., Thornton, J. A., Yatavelli, R. L. N., McKay, M., Goldstein, A. H., LaFranchi, B., ... & Cohen, R. C. (2009). Eddy covariance fluxes of acyl peroxy nitrates (PAN, PPN and MPAN) above a Ponderosa pine forest. *Atmospheric Chemistry and Physics*, *9*(2), 615-634.

Wolff, V., Trebs, I., Foken, T., & Meixner, F. X. (2010). Exchange of reactive nitrogen compounds: concentrations and fluxes of total ammonium and total nitrate above a spruce canopy. *Biogeosciences*, *7*(5), 1729-1744.